1 **Evaluation of Recently-Proposed Secondary Organic Aerosol**

2 **Models for a Case Study in Mexico City**

3 Katja Dzepina[1,2,3], Rainer M. Volkamer[2], Sasha Madronich[3], Pierre Tulet[1,3,4], Ingrid M.
4 Ulbrich[1,2], Qi Zhang[5], Christopher D. Cappa[6], Paul J. Ziemann[7], and Jose L. Jimenez[1,2] [*]
5
6 [1]Cooperative Institute for Research in the Environmental Sciences (CIRES), University
7 of Colorado at Boulder, Boulder, CO
8 [2]Department of Chemistry and Biochemistry, University of Colorado at Boulder,
9 Boulder, CO
10 [3]National Center for Atmospheric Research – Atmospheric Chemistry Division, Boulder,
11 CO
12 [4]Meteo France / CNRM-GREI, Toulouse, France
13 [5]Atmospheric Sciences Research Center, University at Albany, SUNY, Albany, NY
14 [6]Department of Civil and Environmental Engineering, University of California at Davis,
15 Davis, CA
16 [7]Air Pollution Research Center, University of California, Riverside, CA
17
18
19
20 * Corresponding author (email: jose.jimenez@colorado.edu)
21
22
23
24

Supplementary Information Section

Section SI-1: List of abbreviations

27	AMS	Aerodyne aerosol mass spectrometer
28	BBOA	Biomass burning organic aerosols
29	BG-SOA	Background SOA
30	DF	Dilution factor
31	DOAS	Differential optical absorption spectroscopy
32	FTIR	Fourier transform infrared spectroscopy
33	G model	Glyoxal SOA model; uses Volkamer et al. (2007a)
34		parameterization
35	G-SOA	Glyoxal SOA
36	G-SVOC$_g$	Measured gas-phase glyoxal
37	GC-FID	Gas chromatography coupled to flame ionization detector
38	HOA	Hydrocarbon-like organic aerosols
39	IVOC	Intermediate volatility organic compound
40	LIF	Laser induced fluorescence
41	MCMA-2003	Mexico City Metropolitan Area 2003 field campaign
42	MILAGRO-2006	Megacity Initiative: Local and Global Research
43		Observations 2006 field campaign
44	NR-PM$_1$	Non-refractory submicron particulate matter
45	NT model	Non-traditional SOA model; uses Robinson et al. (2007)
46		parameterization
47	NT-P-S/IVOC	Primary emitted S/IVOC in non-traditional SOA model

48	NT-SOA	SOA formed in non-traditional SOA model
49	NT-P-SVOC	Primary emitted SVOC in non-traditional SOA model
50	NT-S-SVOC$_g$	Secondary gas-phase SVOC formed in non-traditional SOA
51		model
52	NT-S-SVOC$_{g+p}$	Total semivolatile (i.e. condensable) material formed in
53		non-traditional SOA model; NT-SSVOC$_{g+p}$ = NT-SOA +
54		NT-SSVOC$_g$
55	OA	Organic aerosols
56	OOA	Oxygenated organic aerosols
57	OOA-1	More aged OOA
58	OOA-2	Fresher OOA
59	PBL	Planetary boundary layer
60	PMF	Positive matrix factorization
61	POA	Primary organic aerosols
62	P-S/IVOC	Primary emitted S/IVOC in non-traditional SOA model
63	Q-AMS	Quadrupole-based Aerodyne aerosol mass spectrometer
64	SOA	Secondary organic aerosols
65	S/IVOC	Semi-volatile and intermediate volatility organic
66		compounds
67	SVOC	Semi-volatile organic compound
68	S/IVOC$_{i,j,g+p}$	Semivolatile material formed in NT model, where i is
69		initial volatility bin, j is the oxidation generation of

70		products from primary emitted S/IVOC, and g and p refers
71		to gas- and particle-phase, respectively.
72	VOC	Volatile organic compound
73	T model	Traditional SOA model; uses only Koo et al. (2003)
74		parameterization
75	T-SOA	SOA formed in traditional model
76	UMR	Unit mass resolution
77	UT model	Updated traditional SOA model; uses Koo et al. (2003)
78		parameterization for all species except for high-yield
79		aromatics for which Ng et al. (2007) parameterization is
80		used
81	UT-pVOC	Secondary product VOC (pVOC) formed in updated
82		traditional model
83	UT-SOA	SOA formed in updated traditional model
84	UT-SVOC$_g$	Secondary gas-phase SVOC formed in updated traditional
85		model
86	UT-SVOC$_{g+p}$	Total semivolatile (i.e. condensable) material formed in
87		updated traditional model; UT-SVOC$_{g+p}$ = UT-SOA + UT-
88		SVOC$_g$
89		

Section SI-2: Additional Support of PMF Results used in This Study

90

91   The HOA spectrum retrieved from PMF (shown in Figures SI-26a) is similar to

92 those of hydrocarbons and has a low oxygen-to-carbon atomic ratio (O/C), and its time

93 series correlates well with combustion tracers such as CO, NO_x, and EC, with ambient

94 ratios (e.g. HOA/CO) consistent with those determined by other methods and studies

95 (Zhang et al., 2005ab; Takegawa et al., 2006; Lanz et al., 2007, 2008; Ulbrich et al.,

96 2008; Aiken et al., 2007, 2008). For these reasons it is interpreted as a surrogate of urban

97 POA. Note that sources such as meat cooking and plastic burning produce AMS spectra

98 very similar to vehicle emissions (Mohr et al., 2008) and thus these and other reduced

99 OA primary sources are likely grouped into HOA by factor analysis.

100   OOA spectra have high oxygen content and show similarities to chamber SOA

101 spectra such as high *m/z* 44 and low signal at higher *m/z* (Figures SI-26b and SI-26c), and

102 typically correlate with photochemical products such as O_3, O_x, glyoxal, and ammonium

103 nitrate during periods dominated by SOA production (Zhang et al., 2005b; Volkamer et

104 al., 2006; Aiken et al., 2008; Herndon et al., 2008). OOA correlates strongly with the

105 SOA estimated with up to four other independent methods (Kondo et al., 2007;

106 Takegawa et al., 2006; Aiken et al., 2009; Docherty et al., 2008). For these reasons OOA

107 is interpreted as an SOA surrogate arising from urban precursors.

108   BBOA correlates well with biomass burning tracers, such as acetonitrile,

109 levoglucosan, elemental potassium and satellite fire counts (Aiken et al., 2008, 2009).

110 The case studies described here were characterized by low regional BB influence (from

111 forest and agricultural fires), as described later in this section, and thus the contribution of

112 regional BB to OOA should be very small. The emitted VOC and SOA formed from

113 urban burning sources such as biofuel use and trash burning are accounted for properly in

114 our analyses, since we use the measured VOC (from all sources) in the model.

115 Primary OA from regional biomass burning (forest and agricultural fires) can be an

116 important contributor to OA concentrations in Mexico City (Salcedo et al., 2006; Molina

117 et al., 2007; Aiken et al., 2009). During MCMA-2003 the regional BB influence was

118 important during the last part of the campaign, from about April 23 to May 4, 2003

119 (Salcedo et al., 2006; Molina et al., 2007). Figure SI-27 shows the time series of several

120 variables and tracers related to biomass burning. The OA concentration is approximately

121   constant (besides a strong diurnal cycle) during the first part of the campaign and then

122   steadily increases during the BB-influenced period, together with the AMS proxy for

123   levoglucosan ("excess" m/z 60; m/z 60 / OA) and consistent with results from PMF. Fine

124   K arises from both biomass burning and dust sources (Johnson et al., 2006; Querol et al.,

125   2008). The concentration of K is smallest at the very beginning of campaign and

126   increases significantly towards the end of the campaign. MODIS satellite fire counts (C.

127   Wiedinmyer, NCAR, pers. comm.) are consistent with these tracers and show very low

128   fire activity in the region around the MCMA from the beginning of April until the later

129   part of the month. Fire counts in all of Mexico also have a minimum in the period April

130   9-14.

131   BB tracers are low during the case study of April 9, 2003, as shown in Figure SI-

132   28. In particular fine K reaches the *lowest value of the field campaign* during our case

133   study, and m/z 60 does not show an enhancement that would be indicative of fire

134   influence. Fire counts in the MCMA and surrounding mountains are zero. The period

135   around our case study was cloudy, which could bias the fire counts low if the thermal

136   signal from a fire is blocked by a cloud. However clouds are also associated with rain and

137   reduced radiation and thus fires are less likely under clouds. We are only aware of one

138   study which has quantified this effect: Schroeder et al. (2008) reported that the

139   probability of fires below clouds in the Amazon was about ¼ - ⅓ of the probability of

140   fires when clouds were absent, indicating that the potential bias of the MODIS fire counts

141   due to cloud presence is small. Taken together these pieces of evidence strongly

142   suggested that our case study was not affected by primary emissions from regional

143   biomass burning.

144   Zinc (Zn) from PIXE measurements is a tracer for industrial emissions in Mexico

145   City. Mass loadings of Zn follow a different pattern than the BB tracers (Johnson et al.,

146   2006), with a minimum during the weekend of the holy week holiday period (April 18-

147   20), consistent with an industrial source. April 9, 2003 shows the highest levels of Zn

148   during MCMA-2003 in the early morning sample (Figure 1d). However, Zn loadings fall

149   to a low value for 12-6 pm, indicating that the industrial emissions associated with high

150   Zn loadings in early morning were not present later in the day, and that the increase is

151   OOA was unrelated to the sources of Zn.

152   Finally, note that if some of the locally-formed SOA arises from precursors

153   emitted from biomass burning sources (either urban or regional), it should be accounted

154   for by our model. Grieshop et al. (2009a) report on chamber aging experiments of wood

155   smoke, and conclude that a traditional SOA model using the measured gas-phase species

156   underpredicts the SOA formed in the aging of biomass burning emissions by a factor of

157   5. The main SOA precursors according to the traditional model are light aromatic and

158   monoterpenes, which are also included in our model. Grieshop et al. (2009a) conclude

159   that the rest of the observed SOA arises from a NT-SOA mechanism, which should also

160   be accounted for in our model since the S/IVOC volatility distribution of wood smoke is

161   similar to that from engine exhaust (Lipsky and Robinson, 2006; Shrivastava et al.,

162   2006).

163 **Supplementary Information References**

164   Alfarra, M.R.: Laboratory and Field Measurements of Organic Aerosols Using the
165   Aerosol Mass Spectrometer; Ph.D. Thesis, University of Manchester Institute of
166   Science and Technology, 2004.
167   Canagaratna, M.R., Jayne, J.T., Ghertner, D.A., Herndon, S., Shi, Q., Jimenez, J.L.,
168   Silva, P.J., Williams, P., Lanni, T., Drewnick, F., Demerjian, K.L., Kolb, C.E., and
169   Worsnop, D.R.: Chase Studies of Particulate Emissions from in-use New York City
170   Vehicles, Aerosol Sci. Tech., 38, 555–573, 2004.
171   Johnson, K.S., de Foy, B., Zuberi, B., et al.: Aerosol composition and source
172   apportionment in the Mexico City Metropolitan Area with PIXE/PESA/STIM and
173   multivariate analysis, Atmos. Chem. Phys., 6, 4591-4600, 2006.
174   Kondo, Y., Miyazaki, Y., Takegawa, N., et al.: Oxygenated and water-soluble organic
175   aerosols in Tokyo, J. Geophys. Res., 112, D01203, doi: 10.1029/2006JD007056, 2007.
176   Lanz, V.A., Alfarra, M.R., Baltensperger, U., et al.: Source attribution of submicron
177   organic aerosols during wintertime inversions by advanced factor analysis of aerosol
178   mass spectra, Environ. Sci. Technol., 42, 214-220, 2008.
179   Querol, X., Pey, J., Minguillón, M.C., Pérez, N., Alastuey, A., Viana, M., Moreno, T.,
180   Bernabé, R.M., Blanco, S., Cárdenas, B., Vega, E., Sosa, G., Escalona, S., Ruiz, H.,
181   and Artíñano, B.: PM speciation and sources in Mexico during the MILAGRO-2006
182   Campaign, Atmos. Chem. Phys., 8, 111-128, 2008.
183   Schroeder, W., Csiszar, I., and Morisette, J.: Quantifying the impact of cloud obscuration
184   on remote sensing of active fires in the Brazilian Amazon, Remote Sensing of
185   Environment, 112, 456–470, 2008.
186

187   **Table SI-1**: Speciation and assumptions of UT model (adapted from Koo et al., 2003 and Ng et al., 2007).

Lumped precursor species name	Measured precursor species	k_{OH} (k_{O3}) (cm^3 molec^{-1} s^{-1})	Stoichiometric SOA yield, α (dimensionless)	$c*$ (300 K) (µg m^{-3})
One-product precursors				
AAR3	Methylcyclopentane Cyclohexane Methylcyclohexane C7-Cycloparaffins n-Heptane, Heptanes isomers n-Octane, Octane isomers n-Nonane, Nonane isomers	8.43×10^{-12}	0.004	1.35
AAR4	>C8-Cycloparaffins n-Decane, Decane isomers Undecane isomers >C12-isomers	1.23×10^{-11}	0.014	1.80
OLE1	Propene 1-Butene 1-Pentene, 1-Pentene isomers 1-Hexene isomers	3.16×10^{-11} (8.92×10^{-18})	0.002	0.90
OLE3	1,3-Butadiene 2-Pentene isomers 2-Hexene isomers Cyclopentene >=Cyclohexene	6.59×10^{-11} (1.21×10^{-16})	0.004	1.12
C7OL	Heptene isomers	6.34×10^{-11} (1.15×10^{-16})	0.013	1.35
C8OL	Octene isomers	6.34×10^{-11} (1.15×10^{-16})	0.035	1.58
C9OL	Nonene isomers	6.34×10^{-11} (1.15×10^{-16})	0.044	1. 58
PHEN	Phenol	$1.63\times10-11$	0.031	1.35

Lumped precursor species name	Measured precursor species	k_{OH} (k_{O3}) (cm^3 molec^{-1} s^{-1})	Stoichiometric SOA yield, α (dimensionless)	c^* (300 K) (µg m^{-3})
One-product precursors – cont.				
BALD	Benzaldehyde Aromatic aldehydes	1.15×10^{-11}	0.0008	1. 58
CRES	Cresols	4.1×10^{-11}	0.034	1.58
ISOP[1]	Isoprene	1.02×10^{-10} (1.28×10^{-17})	0.015	0
Two-products precursors				
TERP	Terpenes	5.37×10^{-11} (8.52×10^{-17})	High-NO$_x$ P1: 0.038 High-NO$_x$ P2: 0.326	3.35 143.2
ARO1[2]	i) Toluene ii) Ethylbenzene i-, n-Propylbenzene i-Butylbenzene o-, m-, p-Ethyltoluene Diethylbenzene isomers	i) 5.96×10^{-12} ii) 9.57×10^{-12};	High-NO$_x$ P1: 0.058 High-NO$_x$ P2: 0.113 Low-NO$_x$: 0.36	2.54 23.28 N/A
BENZ	Benzene	1.23×10^{-12}	High-NO$_x$ P1: 0.072 High-NO$_x$ P2: 0.888 Low-NO$_x$: 0.37	0.33 121.63 N/A
ARO2[2]	i) 1,2,3-, 1,2,4-, 1,3,5- Trimethylbenzene ii) m-xylene iii) p-xylene iv) Styrene v) Naphthalene Methylnaphthalene isomers Other naphthalenes	i) 4.32×10^{-11}; ii) 2.36×10^{-11}; iii) 1.43×10^{-11}; iv) 5.20×10^{-11}; v) 2.30×10^{-11}	High-NO$_x$ P1: 0.031 High-NO$_x$ P2: 0.09 Low-NO$_x$: 0.30	1.44 39.47 N/A

188   ΔH_{vap} for all SOA products, except low-NO$_x$ SOA products, is 36 kJ mol^{-1} (Volkamer et al., 2006). Low-NO$_x$ SOA products are

189   considered non-volatile (c*=0).

190   [1]Isoprene aerosol yields are adopted from Kroll et al., 2005b.

191   [2]ARO1 and ARO2 are defined after original Koo et al. (2003) lumping as AAR5 + toluene, and AAR6 + AAR7, respectively.

192   **Table SI-2**: Assumptions of the NT model (Robinson et al., 2007).

Lumped S/IVOC	Lumped S/IVOC fraction of total (%)	ΔH_{vap} (kJ mol^{-1})	c^* (300 K) (µg m^{-3})
NT-P-S/IVOC$_{1,g+p}$	1.2	112	0.01
NT-P-S/IVOC$_{2,g+p}$	2.4	106	0.1
NT-P-S/IVOC$_{3,g+p}$	3.6	100	1
NT-P-S/IVOC$_{4,g+p}$	5.6	94	10
NT-P-S/IVOC$_{5,g+p}$	7.2	88	100
NT-P-S/IVOC$_{6,g+p}$	12	82	1000
NT-P-S/IVOC$_{7,g+p}$	16	76	10000
NT-P-S/IVOC$_{8,g+p}$	20	70	100000
NT-P-S/IVOC$_{9,g+p}$	32	64	1000000

193   All species are reacting only with OH$^{\cdot}$, with $k_{OH} = 4 \times 10^{-11}$ cm^3 molec^{-1} s^{-1}.

194

195   **Table SI-3**: Gas-particle distribution of primary emissions S/IVOC at different

196   temperatures and OA concentrations.

T (ºC)	c_{OA} (µg m^{-3})	Gas-phase Fraction (%)	Gas-phase / particle-phase Ratio
20	10	87	6.7
20	1	93	13.3
20	0.1	96	24.0
0	10	79	3.8
0	1	87	6.7
0	0.1	92	11.5
-20	10	67	2.0
-20	1	77	3.3
-20	0.1	85	5.7

197

198   **Supplementary Information Figure Captions**

199   **Figure SI-1**: HOA and OOA results from custom principal component analysis method

200   (CPCA; Zhang et al., 2005a) used in Volkamer et al. (2006) and from the PMF method

201   used in this paper.

202   **Figure SI-2**: Size distributions of the selected AMS species during April 9, 2003 for the

203   following time periods: 5 am – 8 am (red), 9 am – 12 pm (yellow), 12 pm – 3 pm (green),

204   and 3 pm – 6 pm (blue).

205   **Figure SI-3**: Data used to calculate primary particle-phase emissions in NT model:

206   temperature (Fig SI-3a), planetary boundary layer (PBL) height (Fig. SI-3b), ratio of the

207   P-S/IVOC mass in gas vs. particle-phase according to the equilibrium calculation with

208   the HOA concentration and temperature and the parameters from Robinson et al. (2007)

209   (SI-6ac), and estimated HOA ("interpolated HOA") (Fig. SI-3d). Also shown in Figure

210   SI-3d are calculated primary emissions per time bin (10 min) ΔHOA. Note that the first

211   point in the ΔHOA time series (Fig. SI-3d) (1.69 μg m^{-3} 10min^{-1}, or ~10% of the total

212   ΔHOA) is to account for the P-S/IVOC in equilibrium with the HOA already present at

213   that point when our simulation starts. The variations in ΔHOA are coming from point-to-

214   point variations in PBL height.

215   **Figure SI-4**: Comparison of the relative time dependence of measured AMS OOA and

216   six different variants of the T and UT models also shown in Fig. 4. The model SOA is

217   multiplied by a different factor in each case in order to allow the evaluation of the relative

218   time dependence.

219   **Figure SI-5**: Parameters related to the calculation of the low- and high-NO$_x$ branching

220   ratio for the UT model. Panel (a): measured NO concentration. Panel (b): measured HO$_2$.

221   concentration. Panel (c): estimated $RO_2\dot{}$ concentration as $RO_2\dot{} = 0.85 * HO_2\dot{}$ (Volkamer

222   et al., 2007b; Sheehy et al., 2008). Panel (d): fraction of $RO_2\dot{}$ reactivity through each of

223   the three possible channels.

224   **Figure SI-6**: Concentrations of lumped model species for UT-SOA (Fig. SI-6a), UT-

225    $SVOC_g$ (Fig. SI-6b) and UT-pVOC (Fig. SI-6c) at 2 pm during our case study.

226   **Figure SI-7**: Comparison of measured OOA and model SOA for selected runs of T

227   model (T_3-SOA and UT_1-SOA) for four other days of MCMA-2003. Also shown are the

228   T_3-SOA and UT_1-SOA results for April 9, 2003 simulations (Fig. 4 of main text).

229   **Figure SI-8**: Concentrations of lumped species from the NT model at 2 pm during our

230   case study. The upper three panels show NT-SOA and the lower three panels show NT-S-

231    $SVOC_g$. The secondary NT-SOA (pink) and NT-S-$SVOC_g$ (blue) are stacked on top of

232   the primary model species NT-POA (gray) and NT-P-S/$IVOC_g$ (dashed gray). Since the

233   distribution of these species is really two-dimensional, we have lumped them in three

234   different ways for one-dimensional representation: the left panels lump the species by the

235   number of oxidation steps undergone, the middle panels by the current saturation

236   concentration of the species, and the right panels by the initial lumped bin of the species

237   (which is directly related to the initial saturation concentration).

238   **Figure SI-9**: Left: evolution of gas- and particle-phase species during April 10, 2003.

239   Right: total model species compared to measured species for April 10, 2003.

240   **Figure SI-10**: Left: evolution of gas- and particle-phase species during April 13, 2003.

241   Right: total model species compared to measured species for April 13, 2003.

242   **Figure SI-11**: Changes in speciation of model SOA and gas-phase species due to

243   evaporation and condensation under equilibrium ("model thermal denuder") for 2 pm

244 species in our case study. Fig. SI-11a and b: UT model species. Fig. SI-11c and d: NT

245 model species binned by current volatility.

246 **Figure SI-12**: Results of kinetic evaporation calculation for model thermal denuder when

247 evaporation coefficient is decreased from 1 (base-case) to 0.1, 0.01 and 0.001. Each panel

248 compares the model base-case kinetic (Fig. 9a) and equilibrium (Fig. 9b) calculations to

249 the kinetic calculations with evaporation coefficients 0.1, 0.01 and 0.001. Fig. SI-12a: NT

250 model POA; Fig. SI-12b: total model SOA; Fig. SI-12c: NT model SOA; Fig. SI-12d: UT

251 model SOA.

252 **Figure SI-13**: Results of kinetic evaporation calculation for model thermal denuder. Left:

253 results when ΔH_{vap} of UT model is changed to 100 kJ mol^{-1}. Right: results when ΔH_{vap} of

254 NT model is changed to 36 kJ mol^{-1}.

255 **Figure SI-14**: Results of kinetic calculation for model thermal denuder for different

256 residence times: 3s (left) and 22s (right).

257 **Figure SI-15**: Results of kinetic evaporation calculations with evaporation coefficient = 1

258 for changing particle size for ± 200 nm. Fig. SI-15a: NT model POA; Fig. SI-15b: total

259 model SOA; Fig. SI-15c: NT model SOA; Fig. SI-15d: UT model SOA.

260 **Figure SI-16**: Volatility basis set representation of NT-SOA and its O/C ratio at four

261 times during the case study.

262 **Figure SI-17**: Changes in model species upon dilution for species present at 2 pm during

263 our case study. Fig. SI-17a and b: UT model species. Fig. SI-17c and d: NT model

264 species binned by current volatility.

265 **Figure SI-18**: Results of alternative dilution case study when the background SOA

266 concentration is zero.

267 **Figure SI-19**: Results of alternative dilution case study when the background SOA

268 concentration is 1 µg m^{-3}.

269 **Figure SI-20**: Changes in model species upon aging without dilution, starting with the

270 speciation at the end of our case study at 2 pm. Left panels: UT model species. Right

271 panels: NT model species binned by current volatility.

272 **Figure SI-21**: Results of sensitivity studies of the NT model when different amounts of

273 IVOC are specified. Upper panels: SVOC : IVOC = 1 : 1 (left: SOA; right: gas-phase

274 species). Middle panels: SVOC : IVOC = 1 : 3. Bottom panels: SVOC : IVOC = 1 : 1.5

275 (base case).

276 **Figure SI-22**: Model SOA base case results with the updated NT model parameters

277 (Grieshop et al., 2009a).

278 **Figure SI-23**: Volatility of each model SOA as well as total model SOA in kinetic

279 calculation for the updated NT model parameters (Grieshop et al., 2009a).

280 **Figure SI-24**: Atomic O/C ratios for model SOA species with the updated NT model

281 parameters (Grieshop et al., 2009a). The error bar shows the estimated uncertainty of

282 measured OOA O/C ratio of ± 30% (Aiken et al., 2007, 2008).

283 **Figure SI-25**: Comparison of (a) the PBL evolution, (b) model SOA and (c) gas-phase

284 SVOC during our base case, and for the following PBL sensitivity studies: i) PBL

285 calculated with the WRF model (A. Hodzic, NCAR, pers.comm., 2008); ii) as in the base

286 case but with maximum PBL height decreased for 800 m; and iii) as in the base case but

287 with maximum PBL height increased for 800 m.

288 **Figure SI-26**: Comparison of spectra from PMF output and characteristic spectra from

289 the AMS spectral database (Ulbrich et al., 2008). Fig. SI-26a: AMS database spectrum of

290   diesel exhaust (Canagaratna et al., 2004) vs. HOA spectrum from our case study. Fig. SI-

291   26b: AMS database spectrum of fulvic acid (Alfarra, 2004) vs. OOA-1 spectrum from

292   our case study. Fig. SI-26c: AMS spectrum of SOA from toluene photooxidation (Aiken

293   et al., 2008) vs. OOA-2 spectrum from our case study.

294   **Figure SI-27**: (a) Time series for all of the MCMA-2003 campaign for the following

295   variables: AMS total OA, AMS proxy for levoglucosan ("excess m/z 60", m/z 60 / OA),

296   MODIS satellite daily fire counts in the region encompassing the MCMA and the

297   surrounding mountains and all of Mexico, and PIXE elemental potassium (K) and zinc

298   (Zn) from two impactor stages that capture particles in the size range 70-1150 nm.

299   **Figure SI-28**: (a) Time series during the period of April 9, 2003 case study for the

300   following variables: AMS total OA, AMS proxy for levoglucosan ("excess m/z 60", m/z

301   60 / OA), MODIS satellite daily fire counts in the region encompassing the MCMA and

302   the surrounding mountains and all of Mexico, and PIXE elemental potassium (K) and

303   zinc (Zn) from two impactor stages that capture particles in the size range 70-1150 nm.

304

305

Evaluation of New Secondary Organic Aerosol Models for a Case Study in Mexico City

Katja Dzepina, Rainer M. Volkamer, Sasha Madronich, Pierre Tulet, Ingrid M. Ulbrich, Qi Zhang, Christopher D. Cappa, Paul J. Ziemann, and Jose L. Jimenez

Supplementary Information Section Figures

Contact author: dzepina@gmail.com
Correspondence author: jose.jimenez@colorado.edu
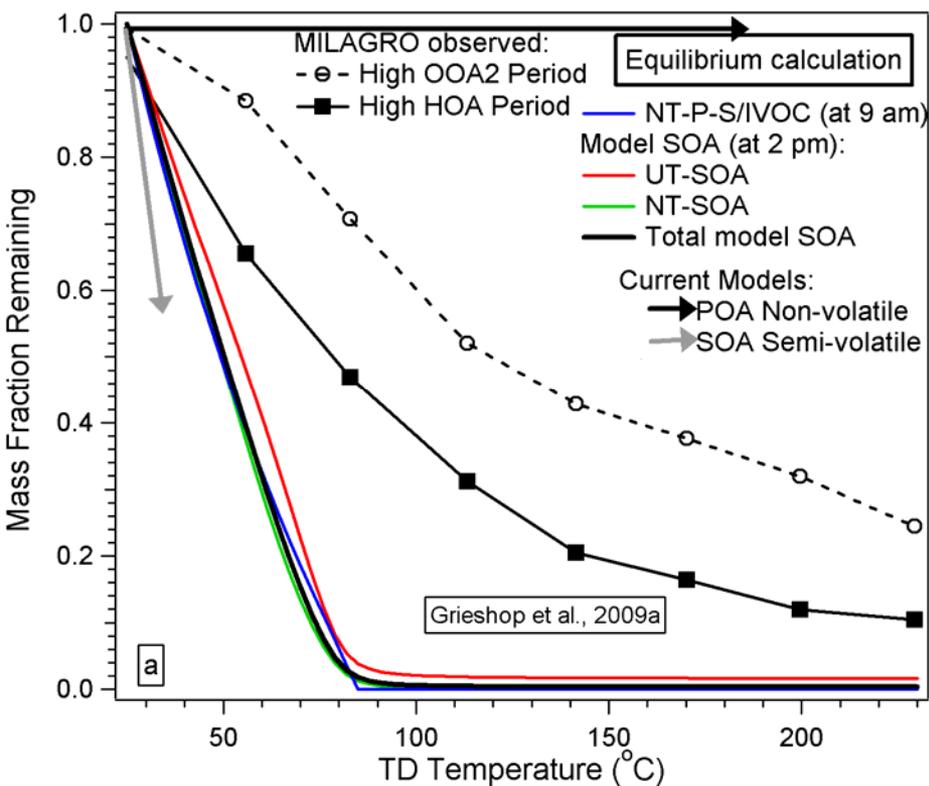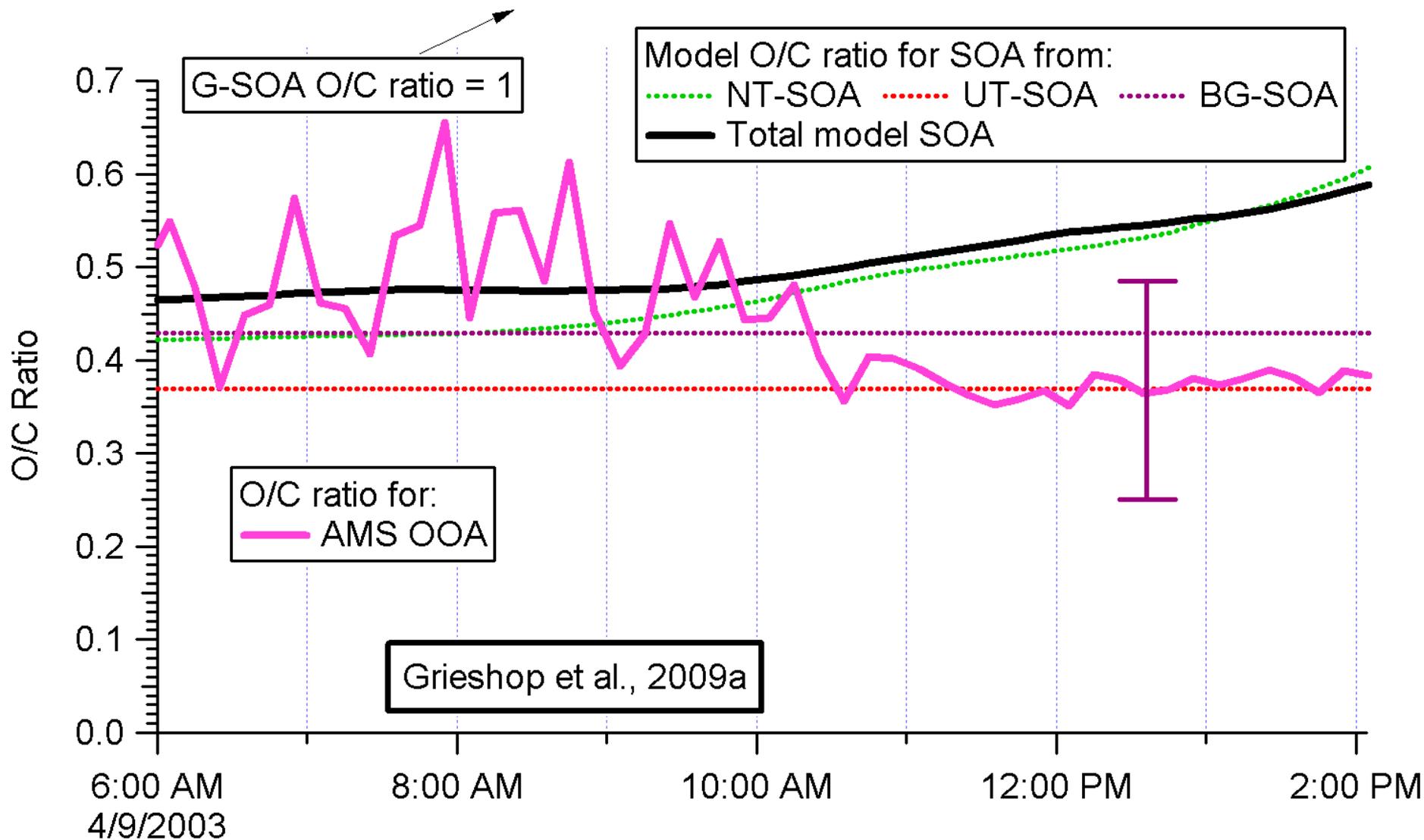
Figure SI-1
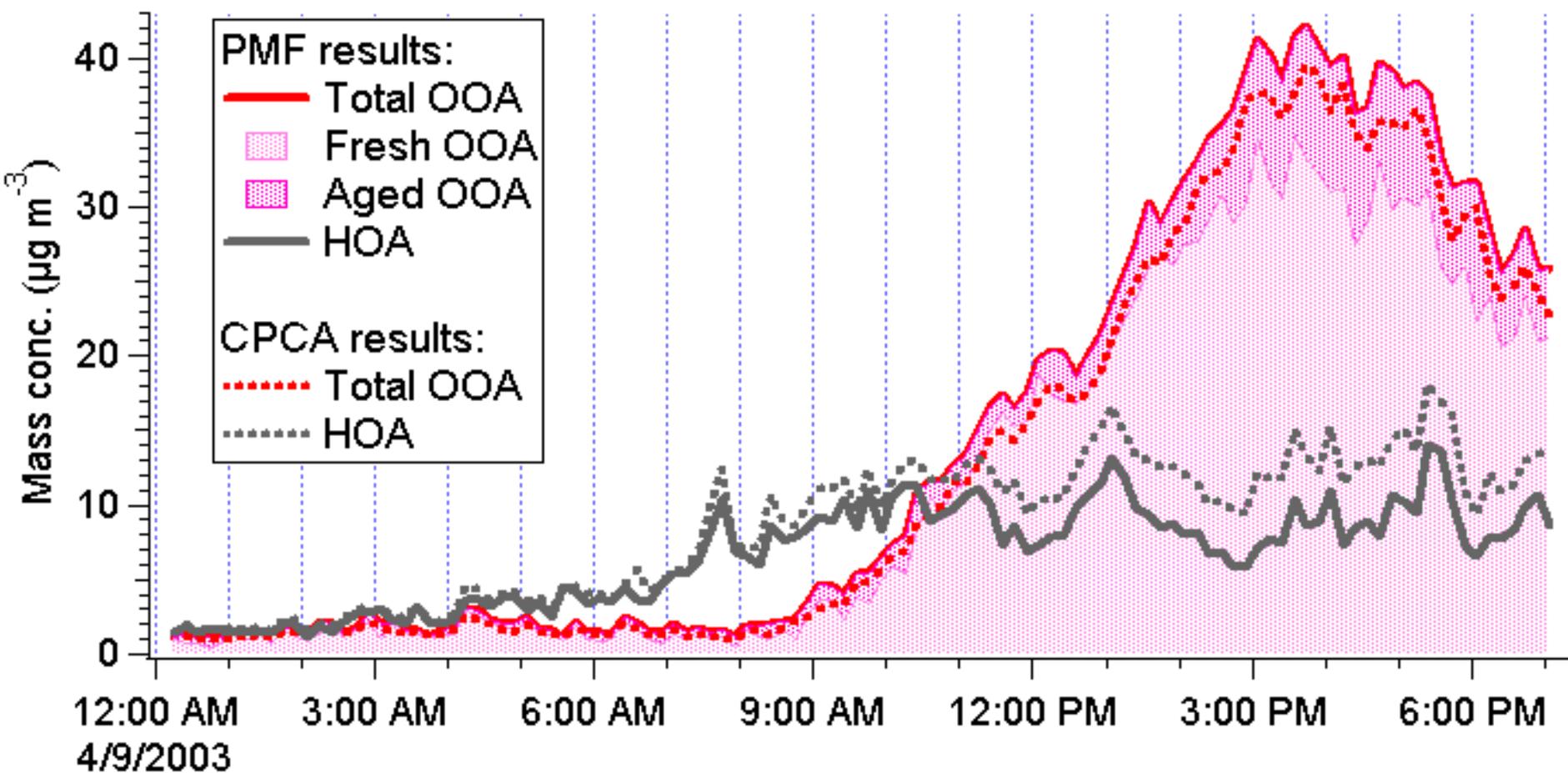
Figure SI-2
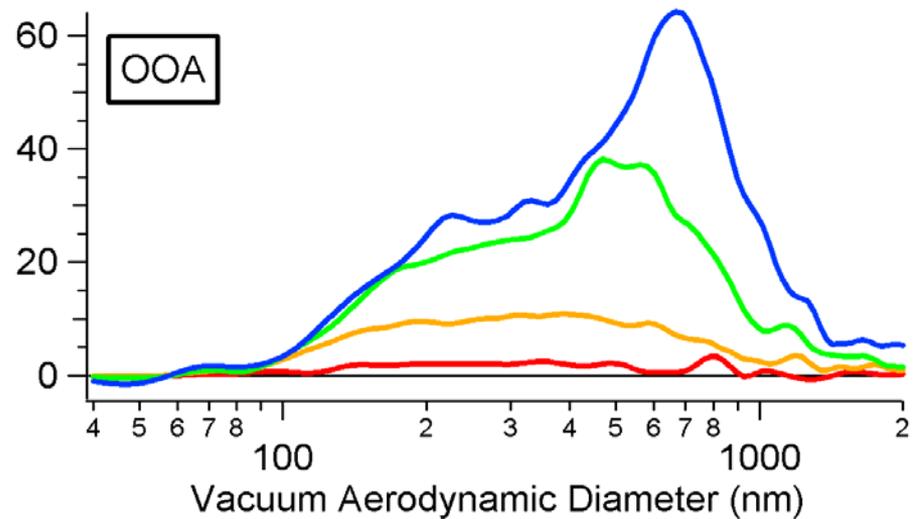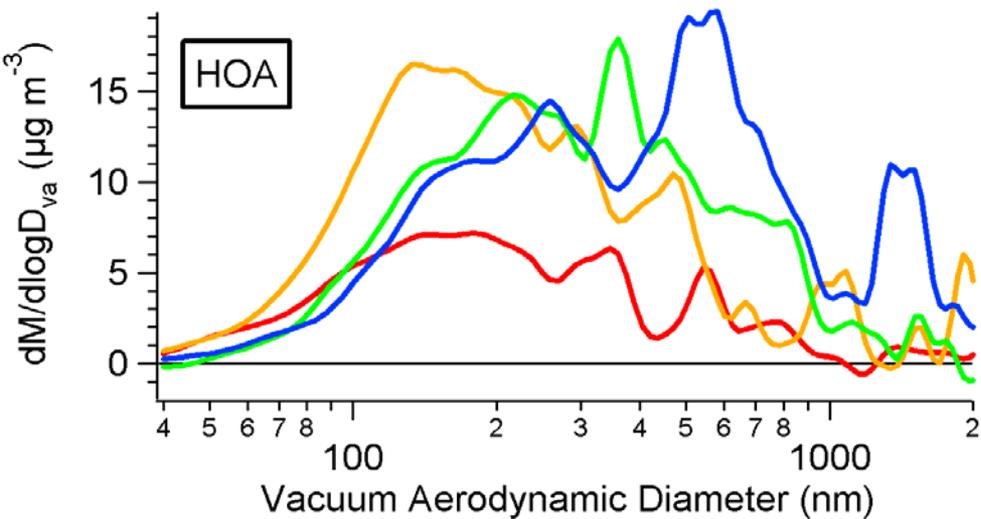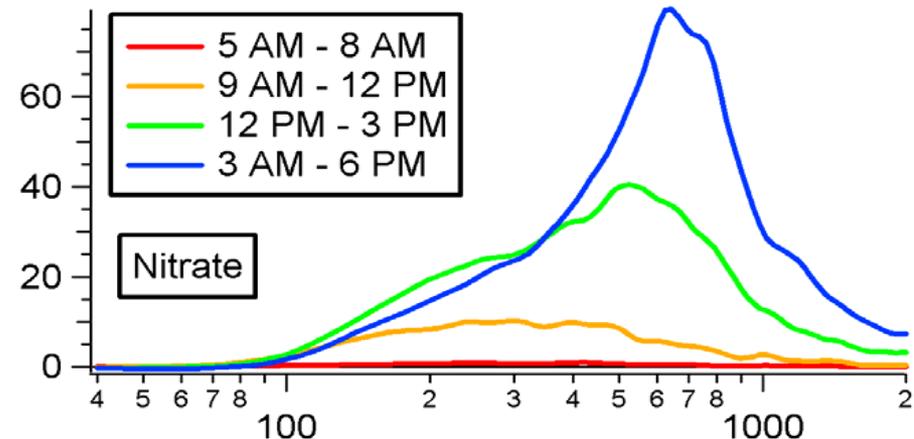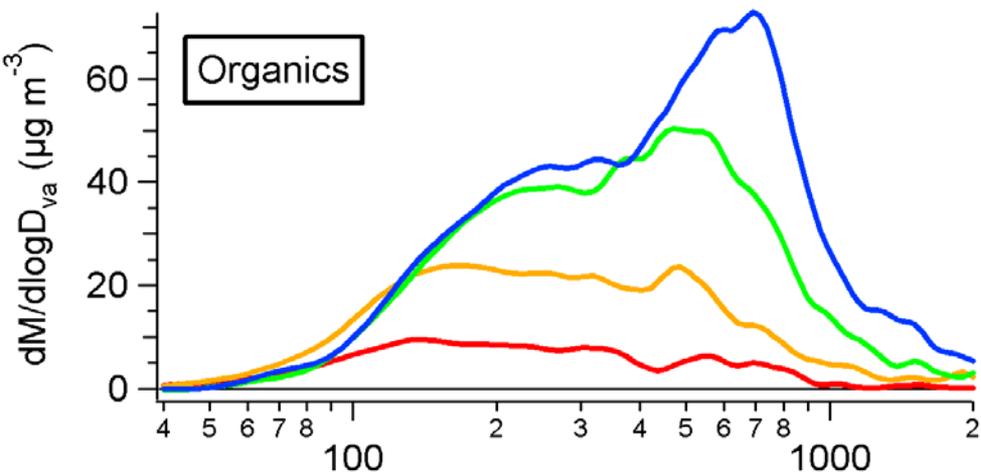
Figure SI-3
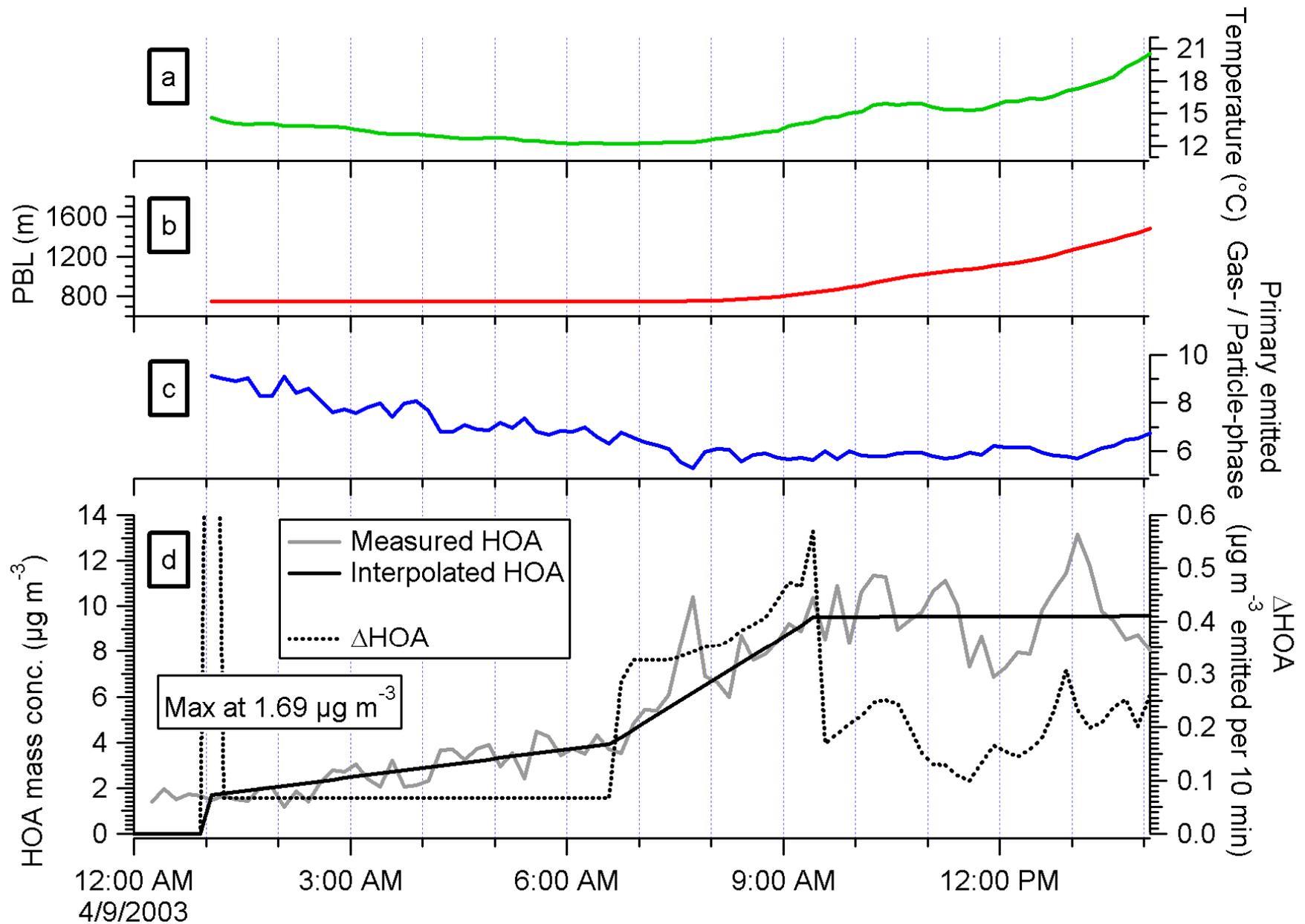
Figure SI-4
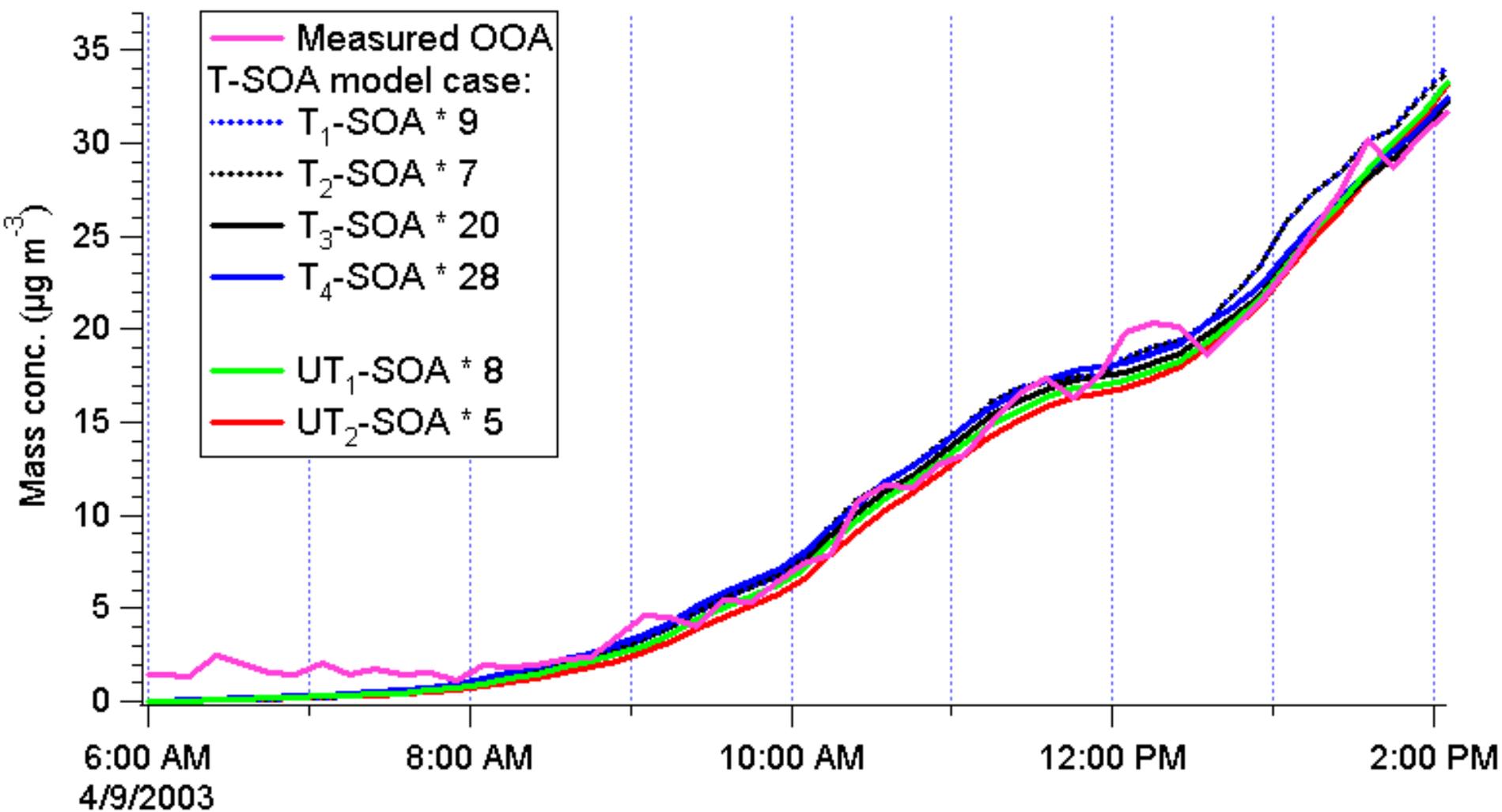
Figure SI-5
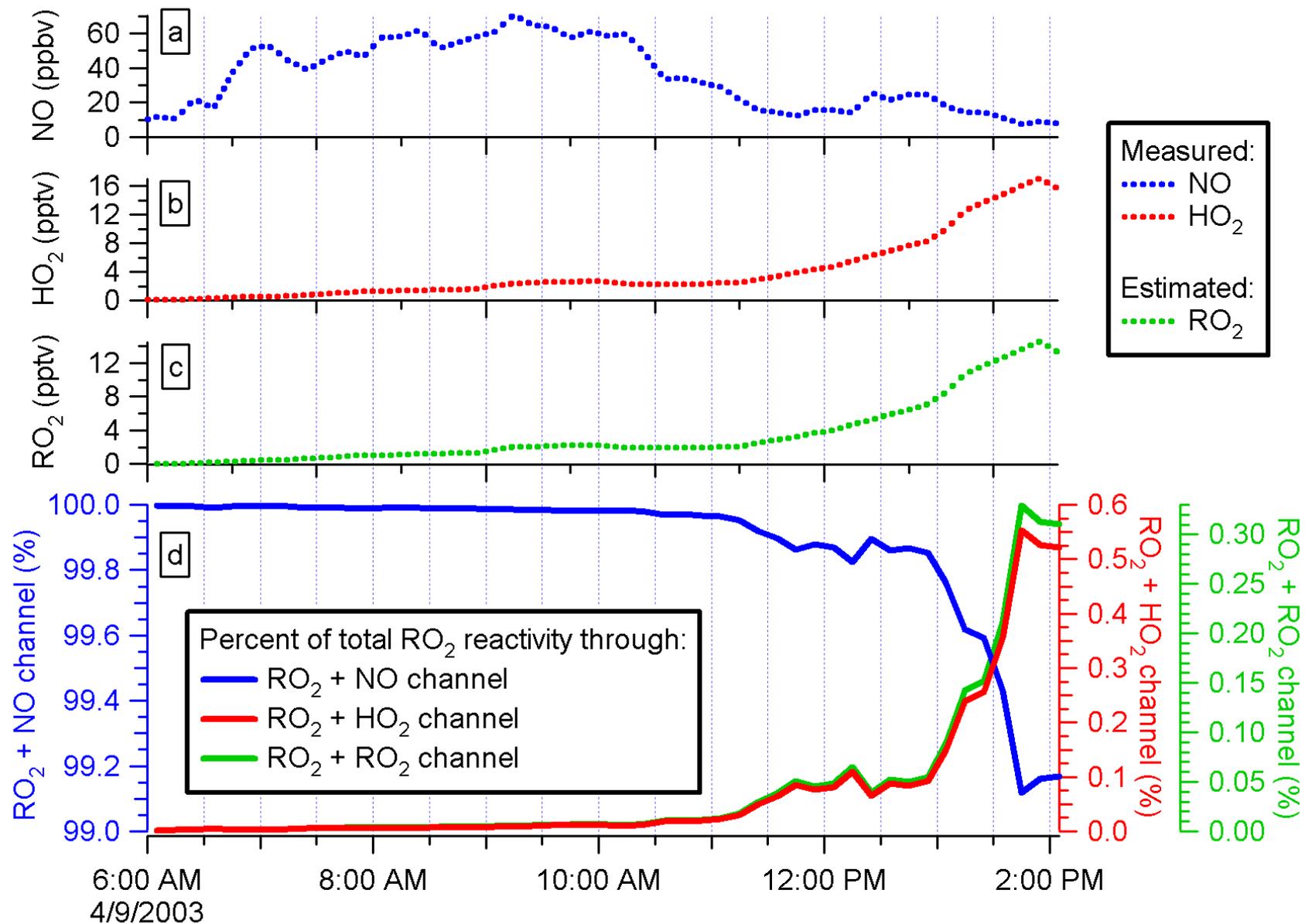
Figure SI-6
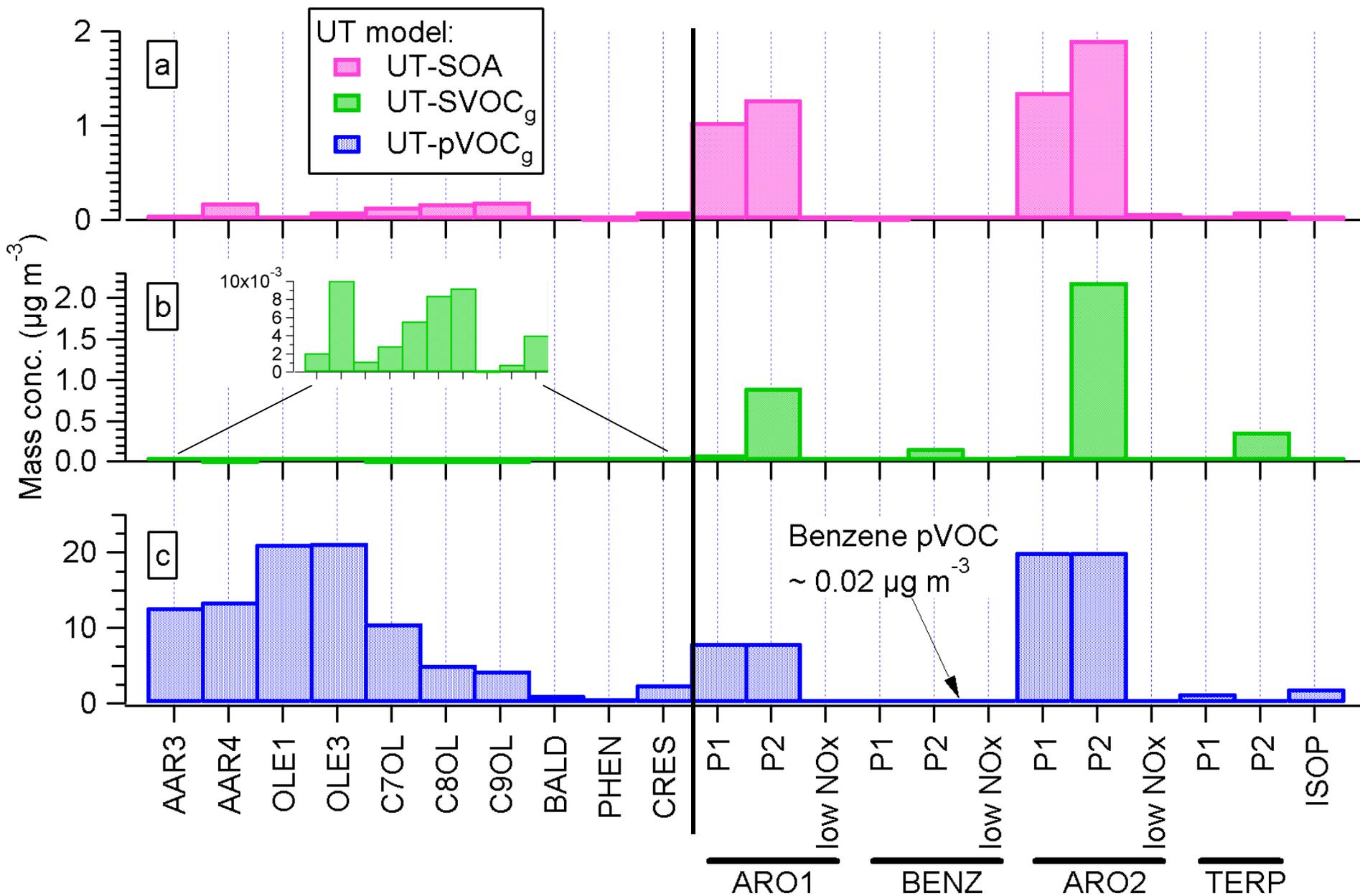
Figure SI-7

Day of MCMA-2003	Meas. OOA / Model SOA @ 10 am	
	T3-SOA case	UT1-SOA case
4/9/2003	8.5	8.3
4/10/2003	9	6.6
4/13/2003	5.2	4
4/14/2003	8.1	5.7
4/22/2003	9.7	7
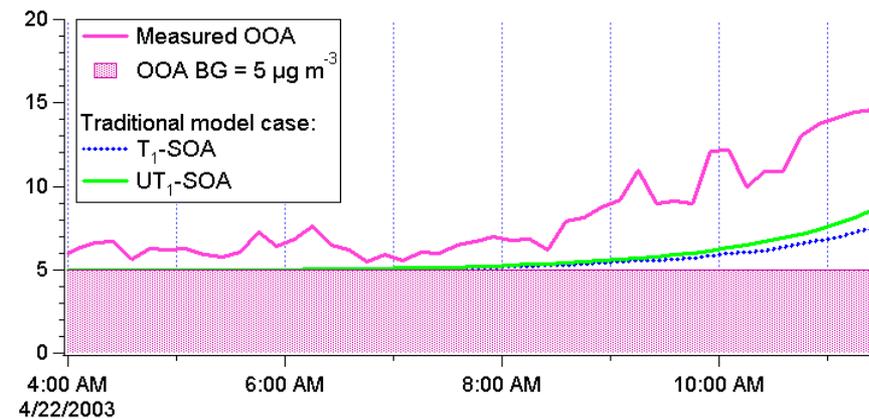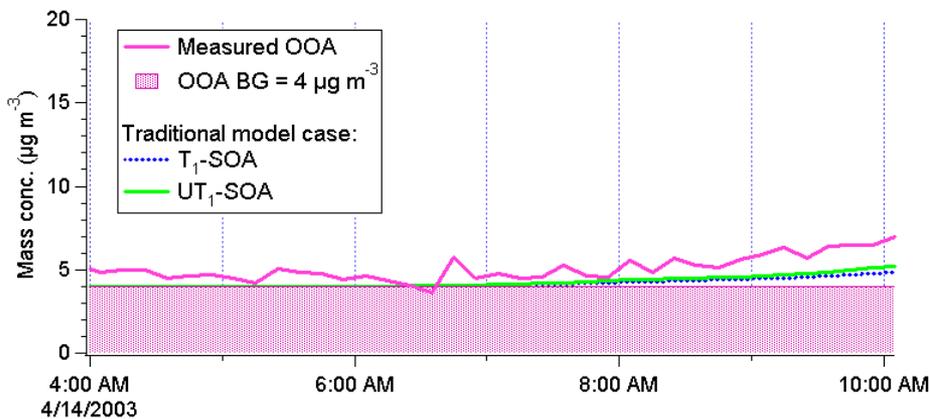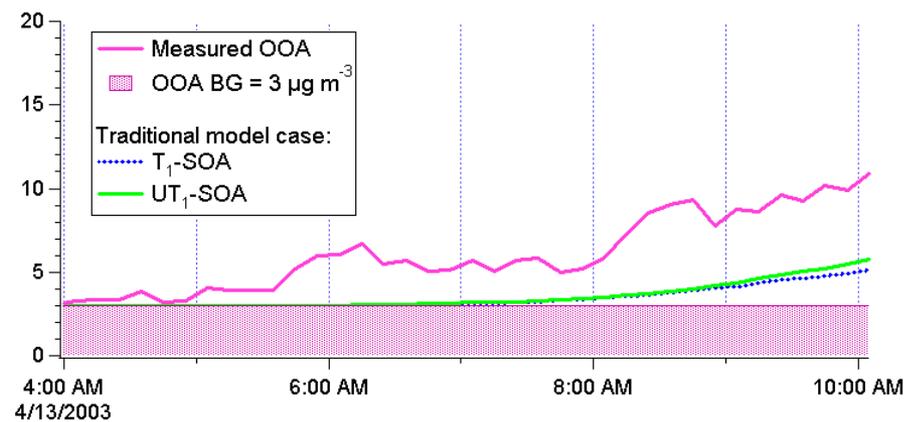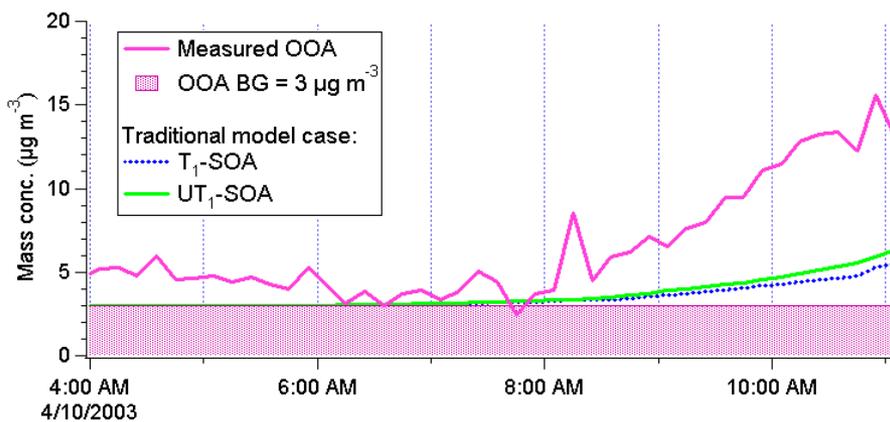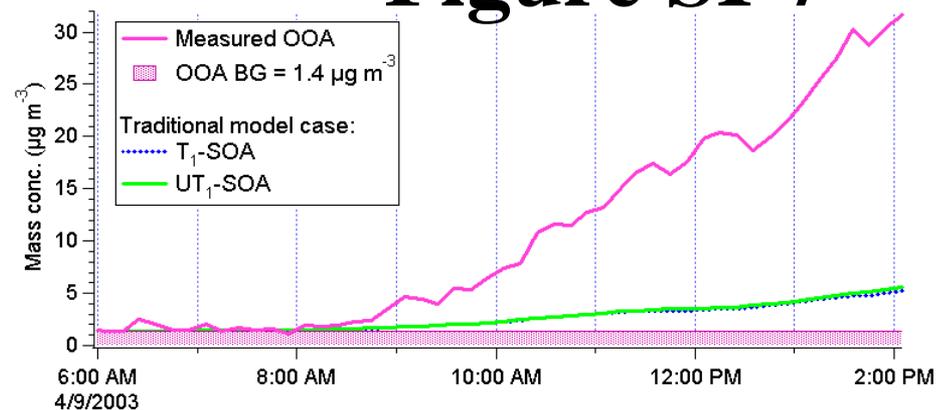
Figure SI-8

Distribution by number of oxidation steps undergone

Distribution by current saturation concentration

Distribution by initial lumped bin of P-S/IVOC

NT-SOA (µg m^{-3})

NT-SVOC$_g$ (µg m^{-3})

NT model 2 pm distribution of:
NT-SOA
NT-SVOC$_g$

NT model 2 pm distribution of:
NT-POA
NT-P-S/IVOC$_g$

From P-S/IVOC$_g$ ox. generation (#)

log c*

From lumped P-S/IVOC bin (#)
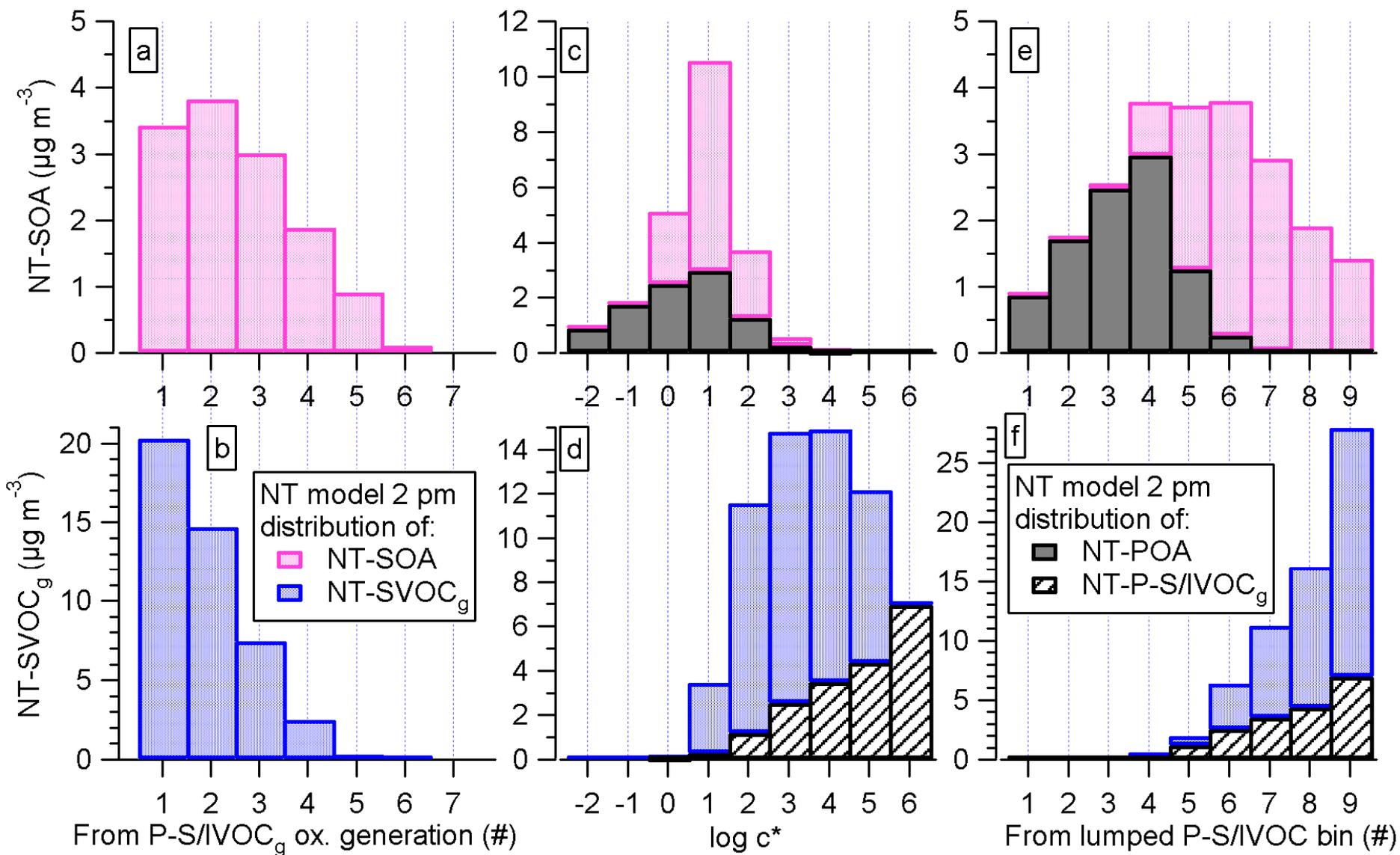
Figure SI-9
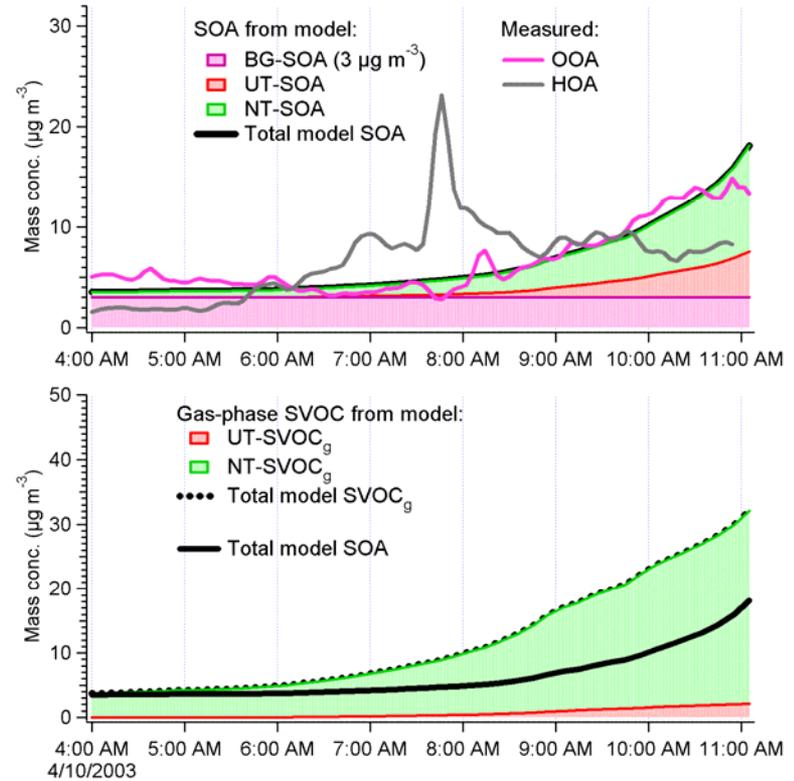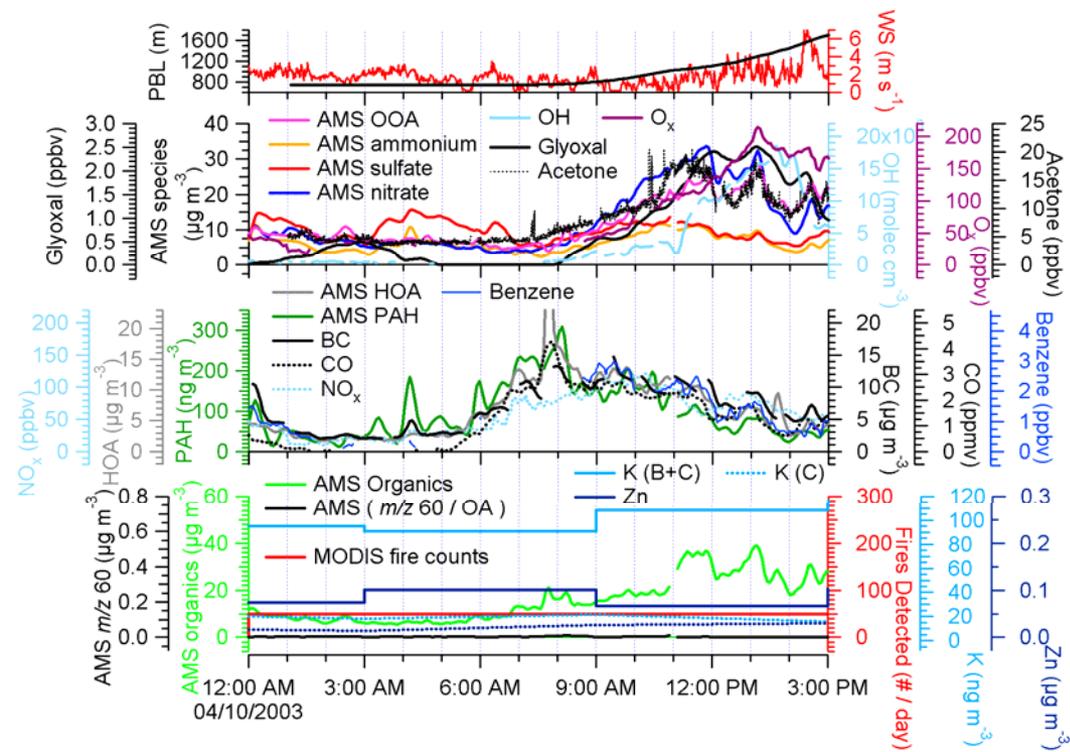
Figure SI-10
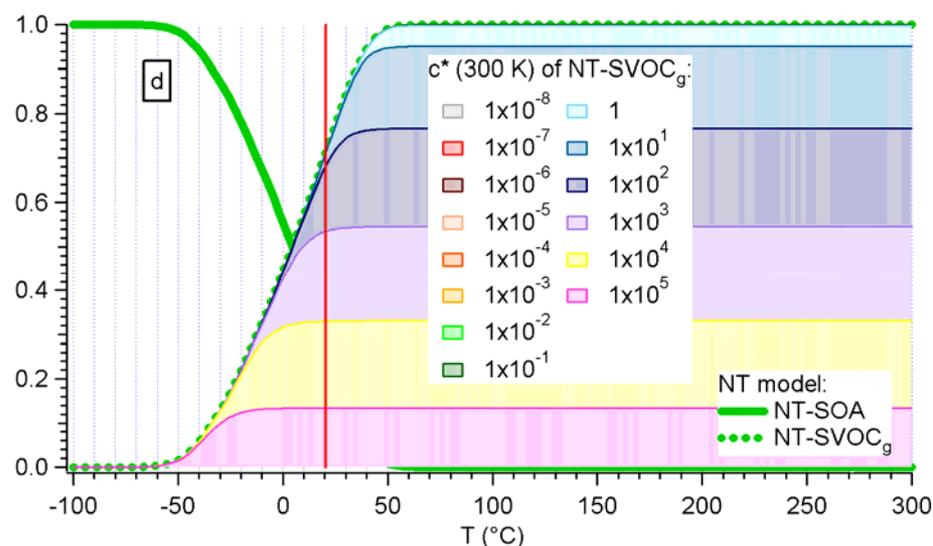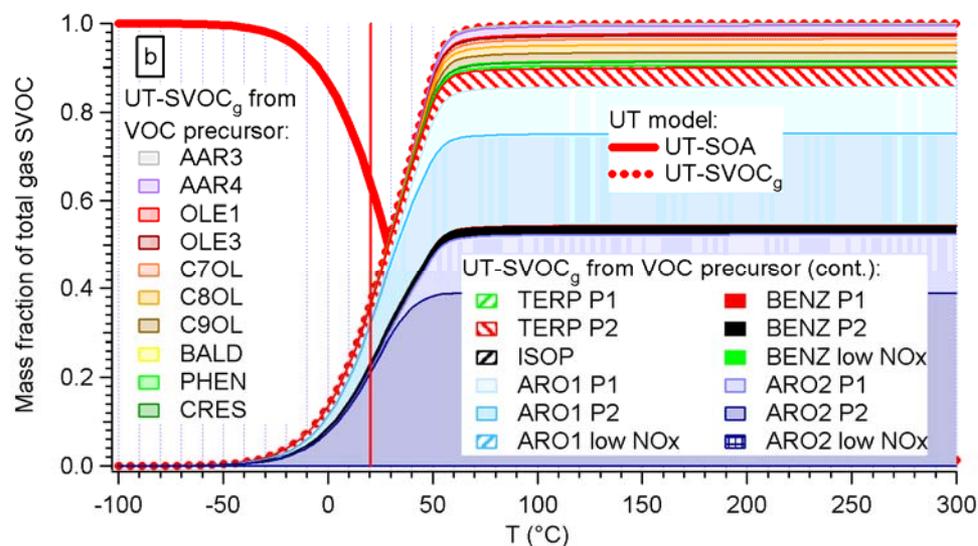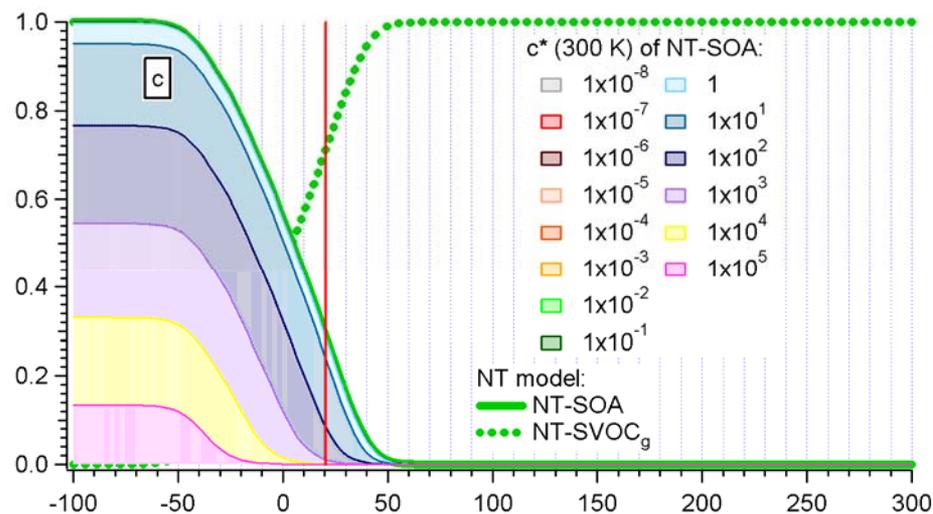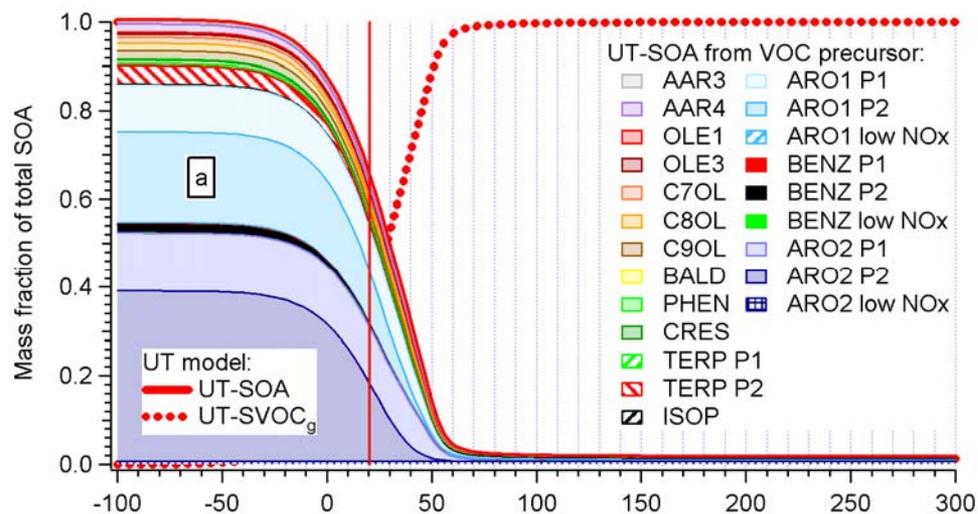
Figure SI-11

Figure SI-12
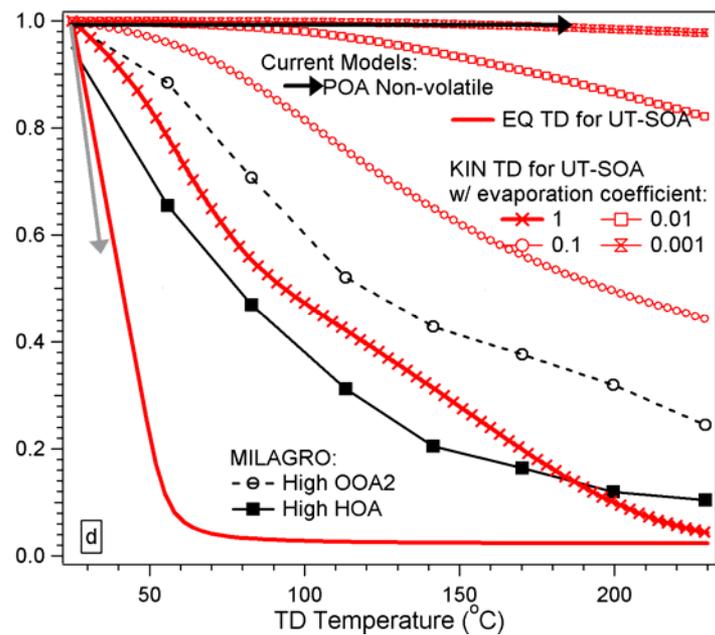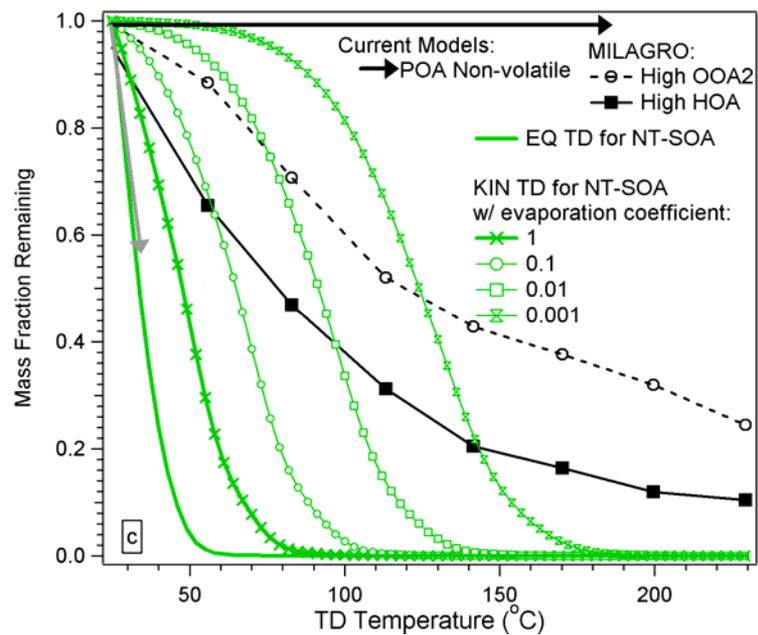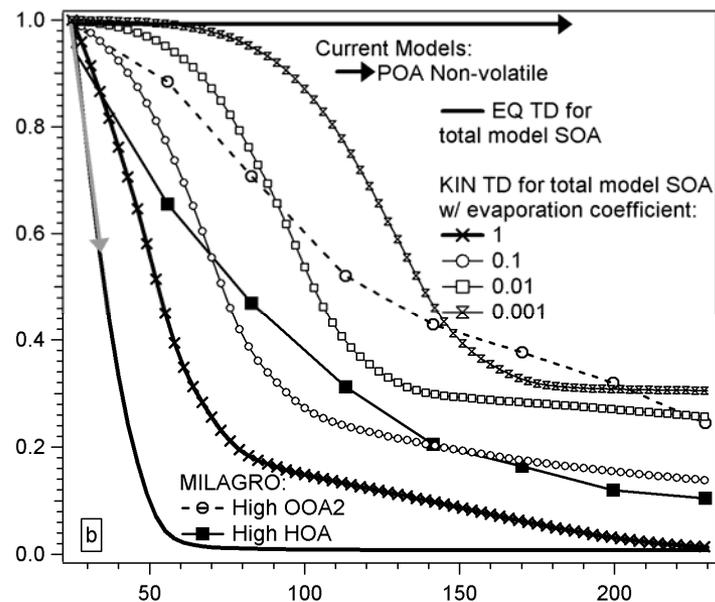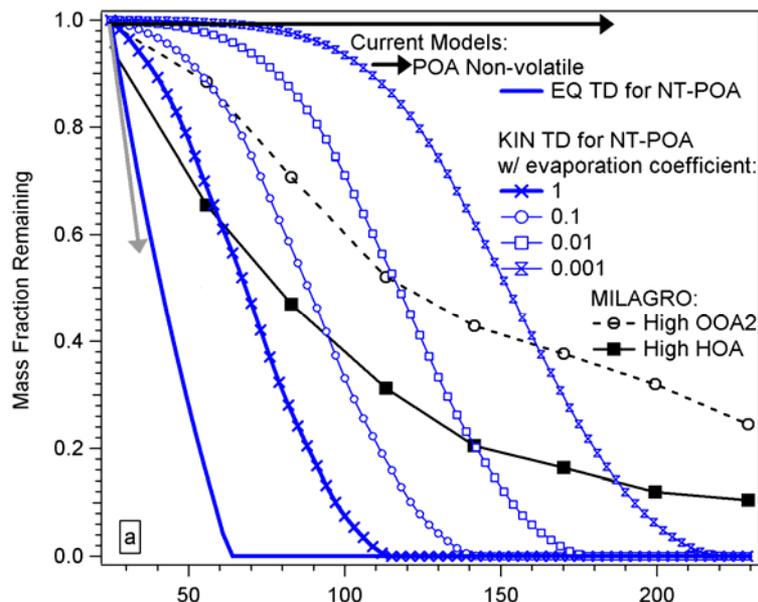
Figure SI-13
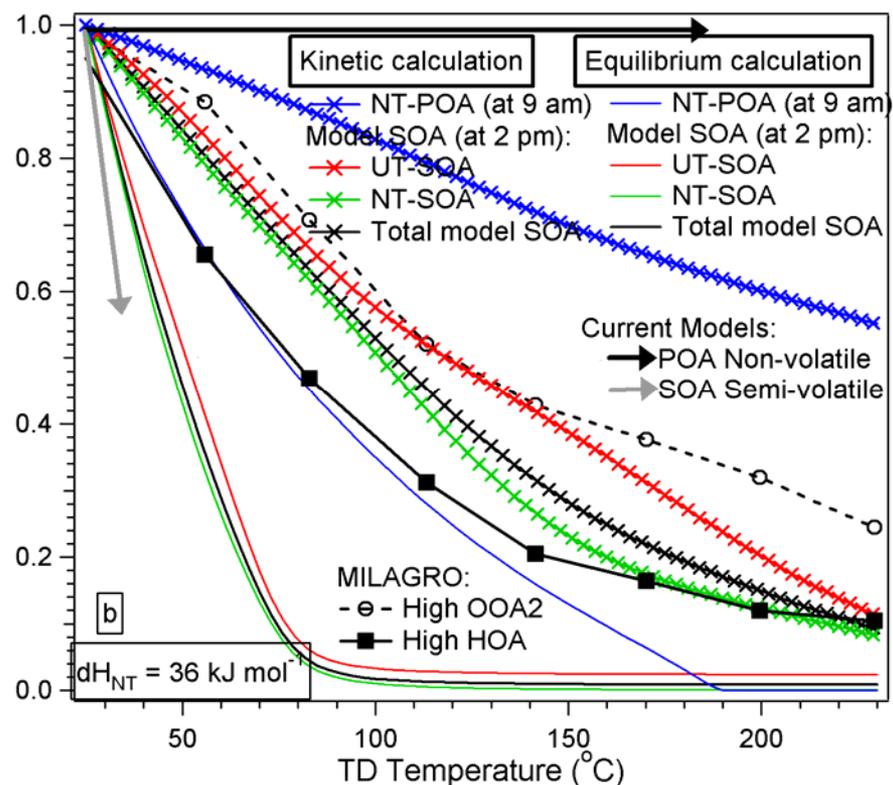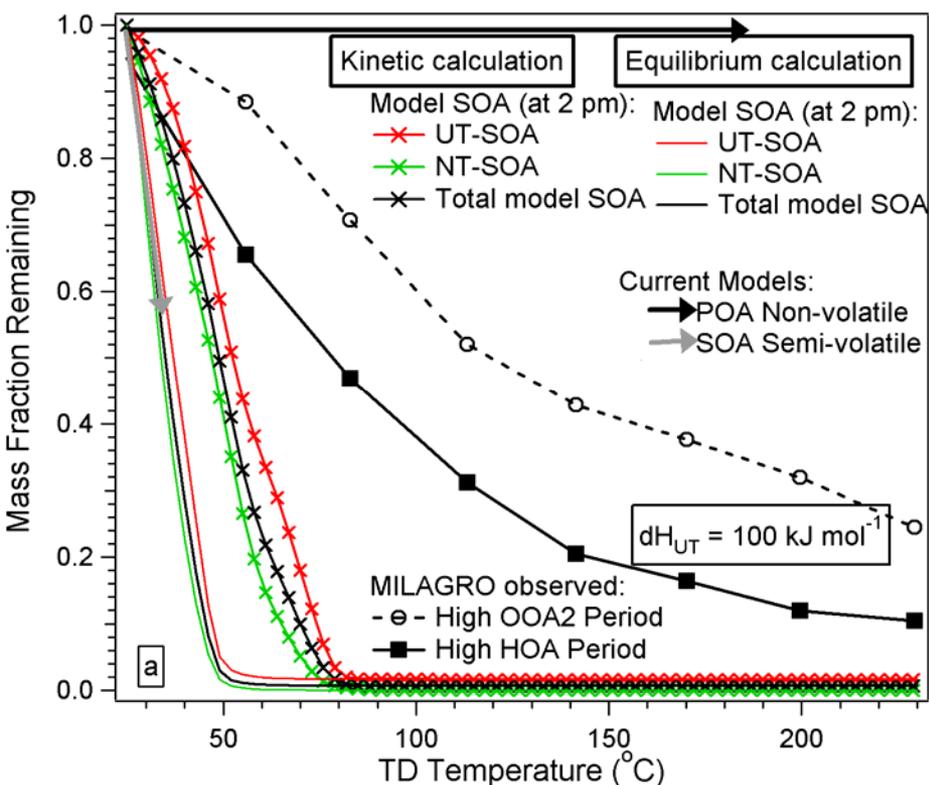
Figure SI-14
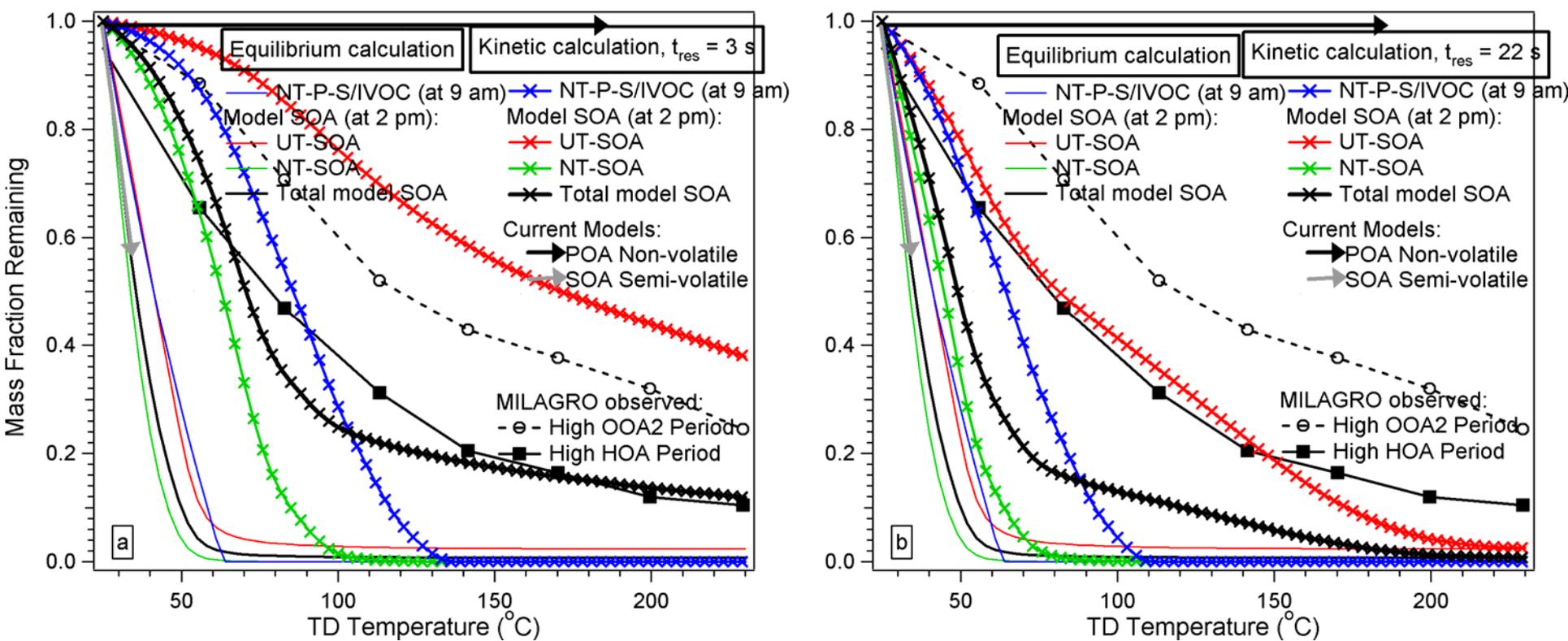
Figure SI-15
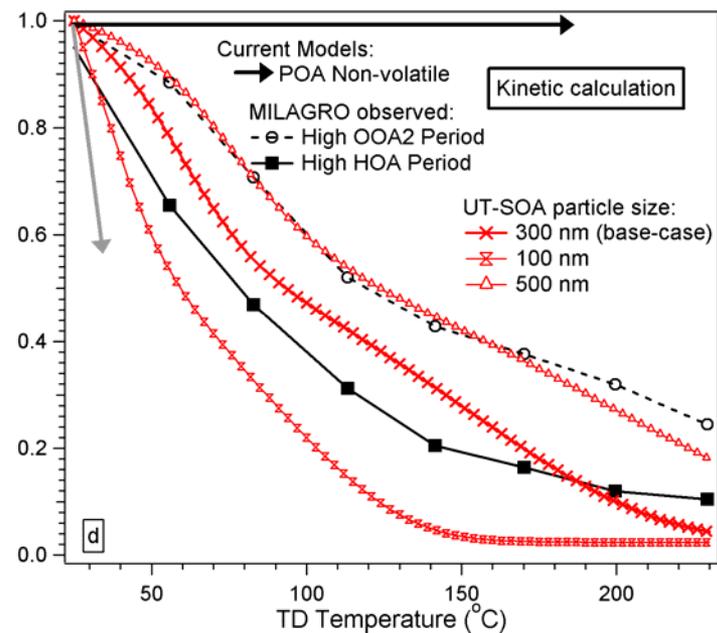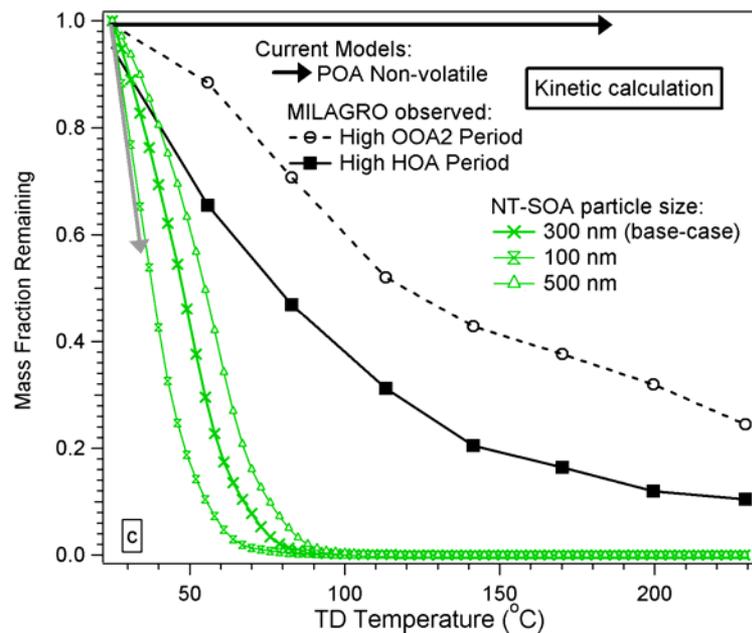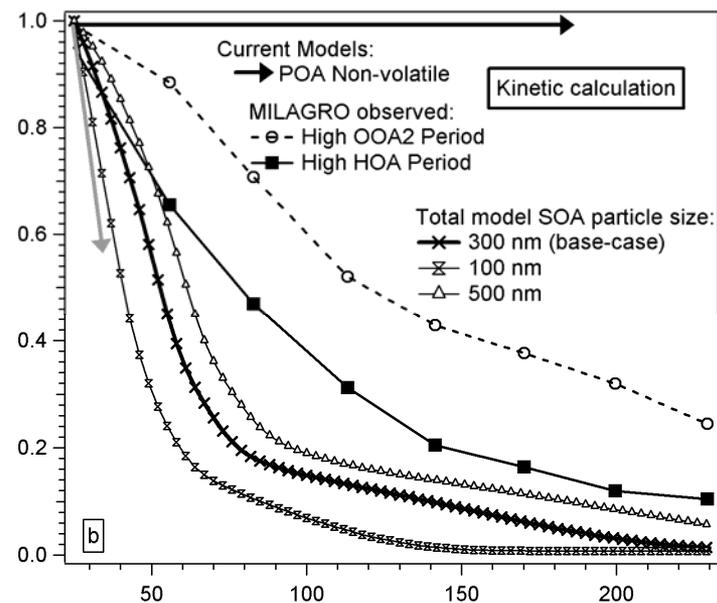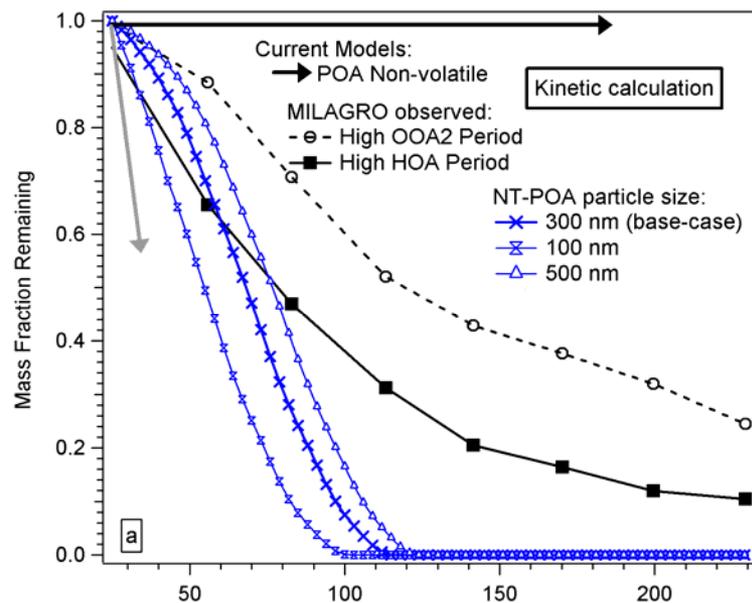
Figure SI-16
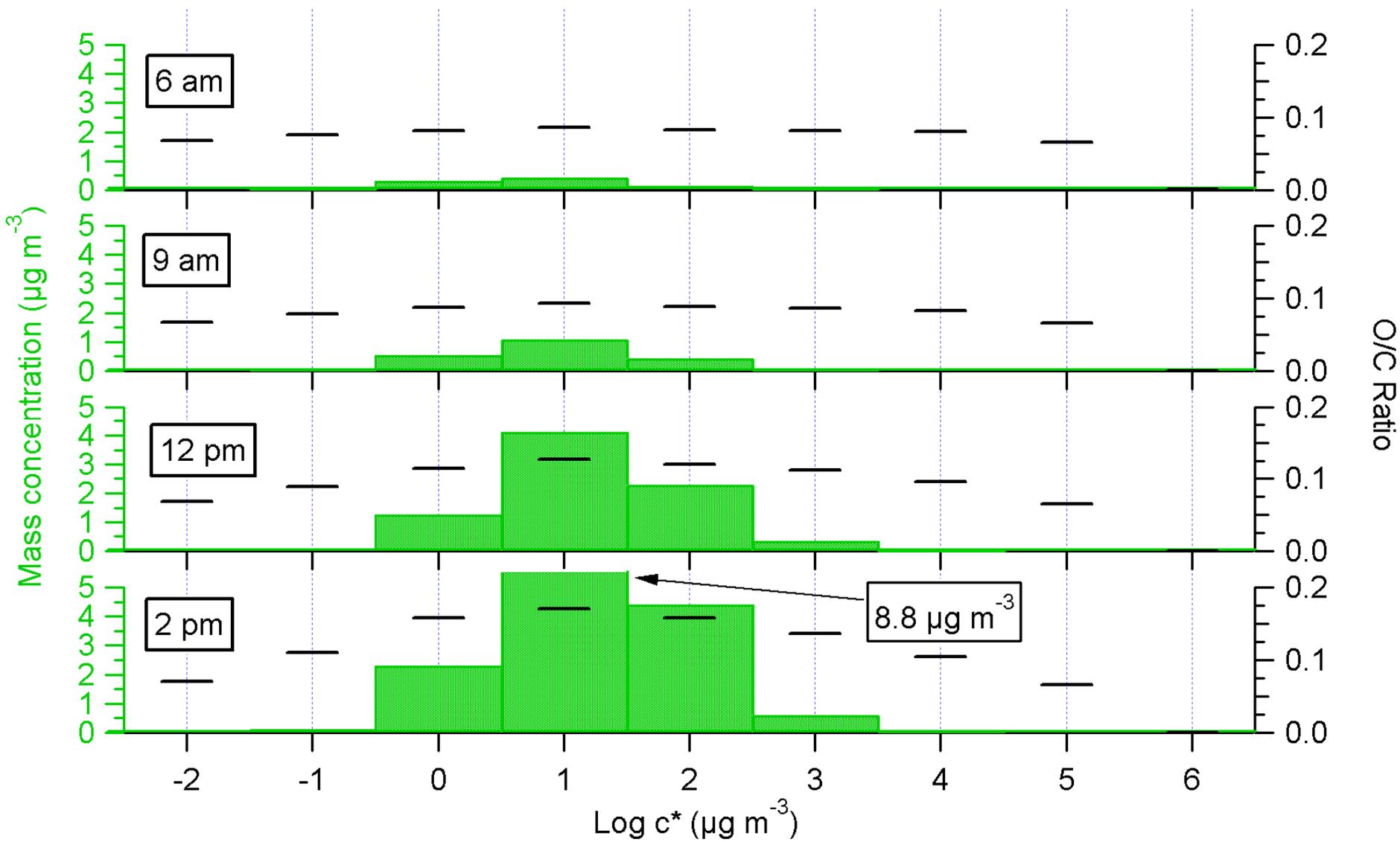
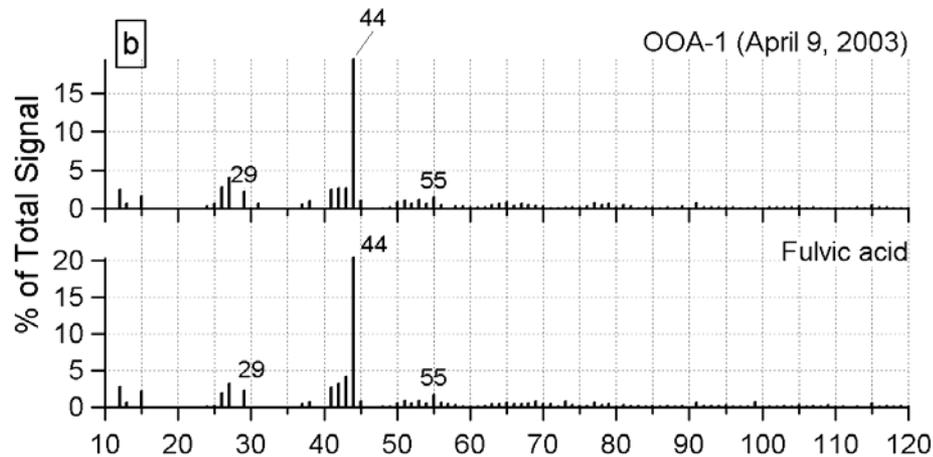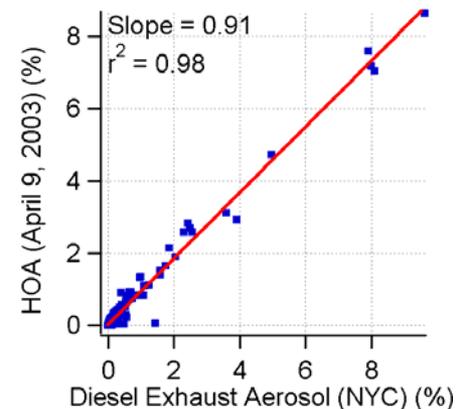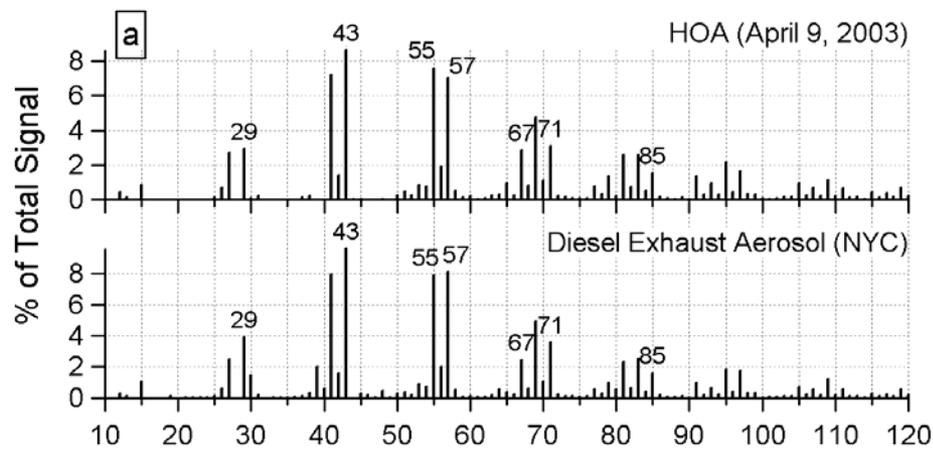# Figure SI-17
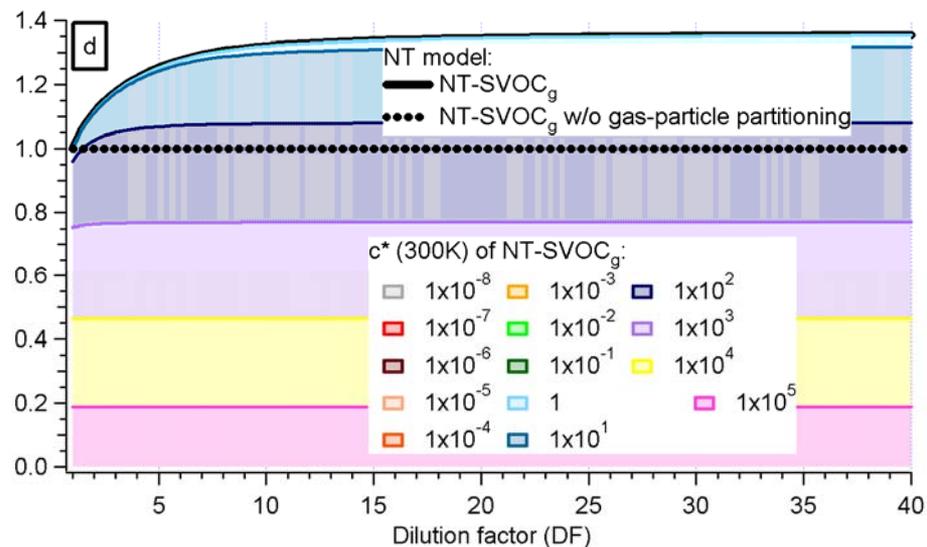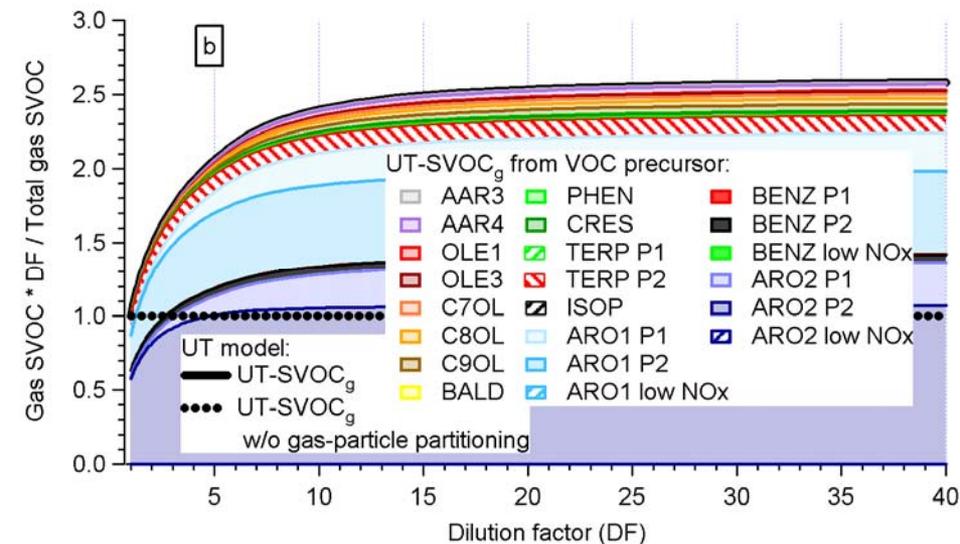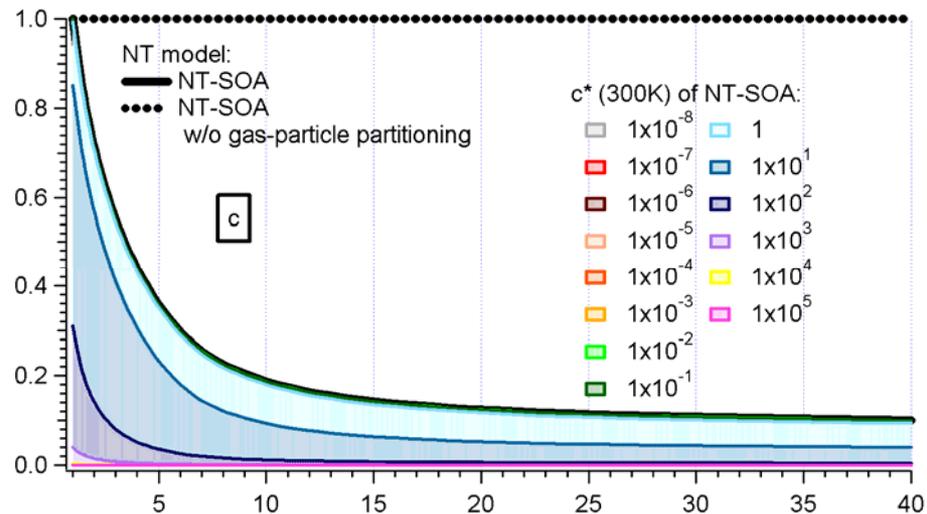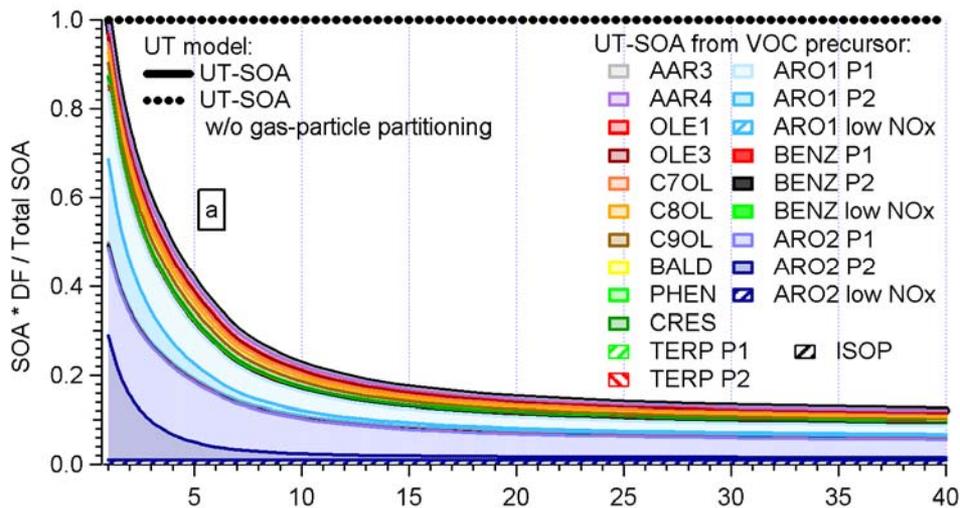
Figure SI-18
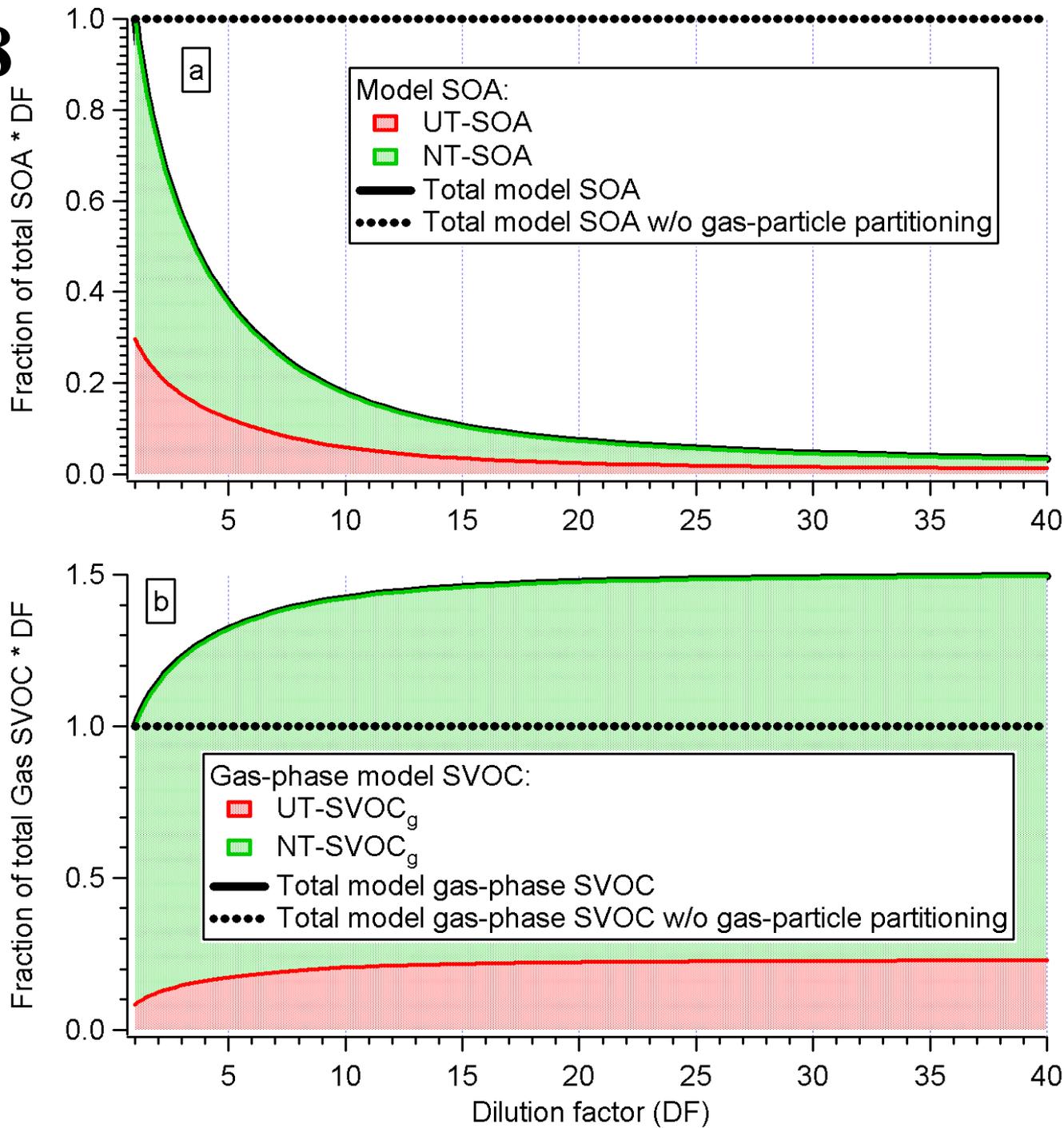
Figure SI-19
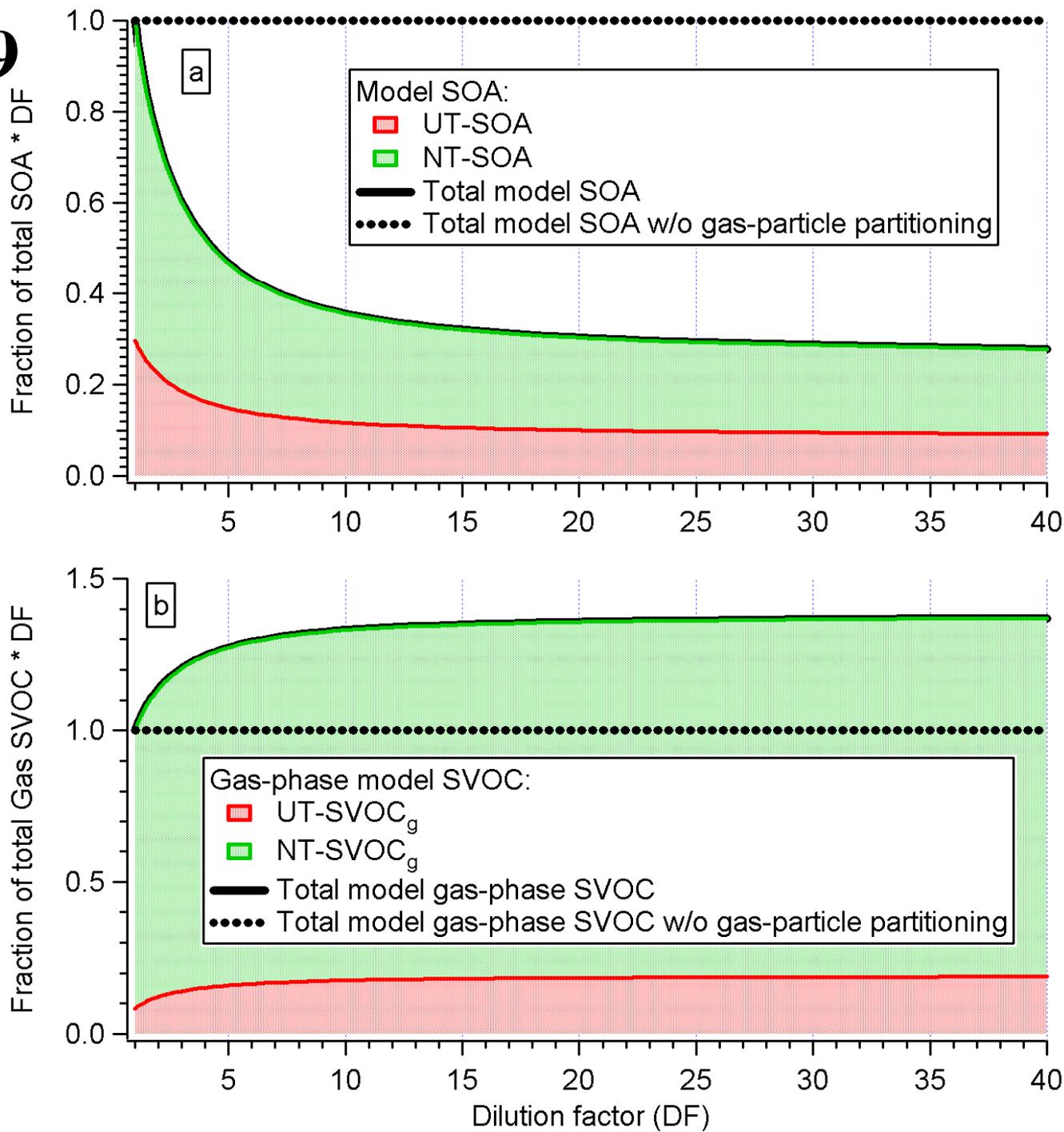
Figure SI-20
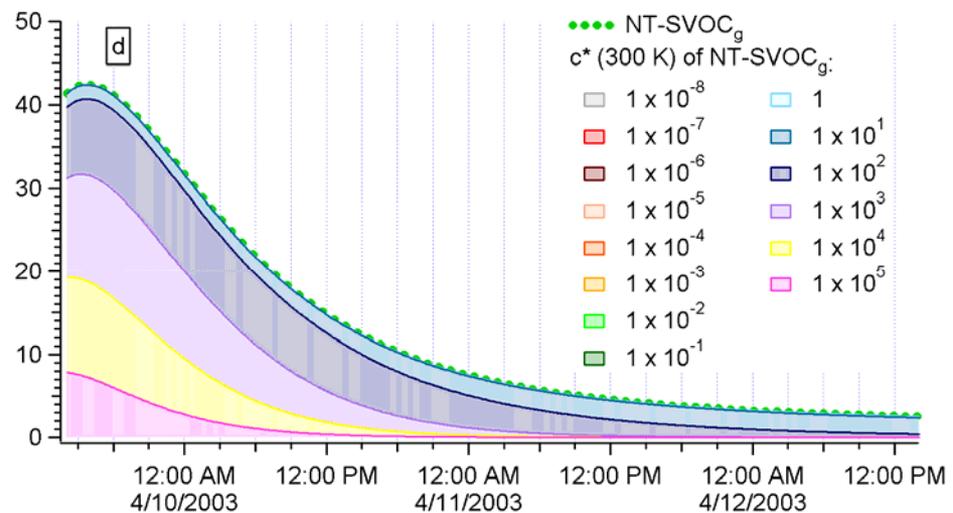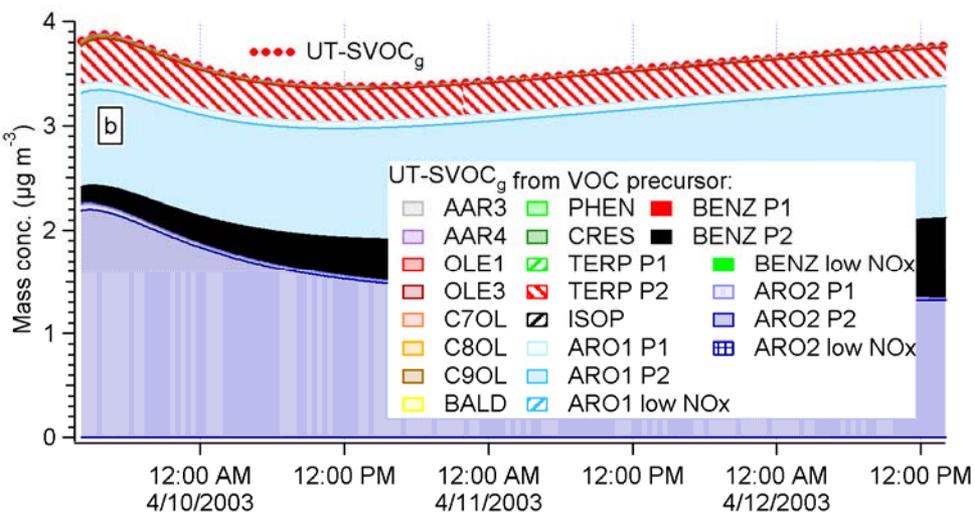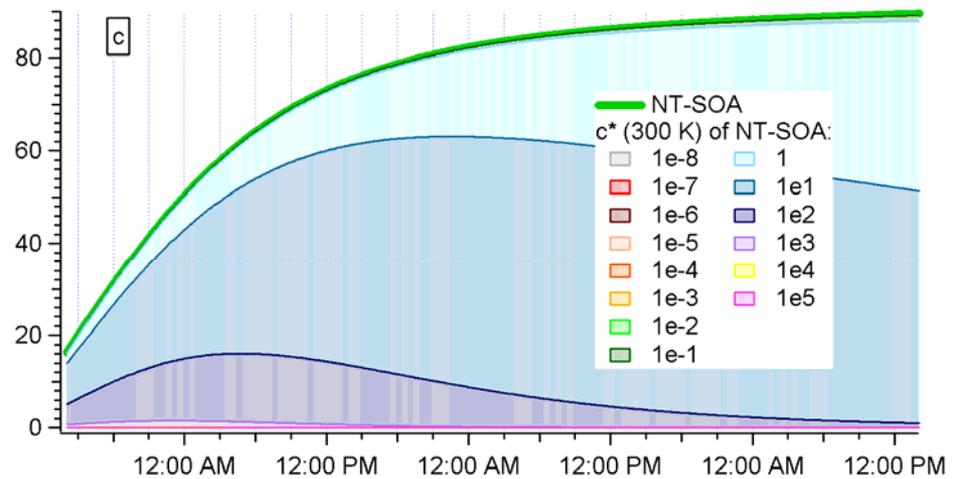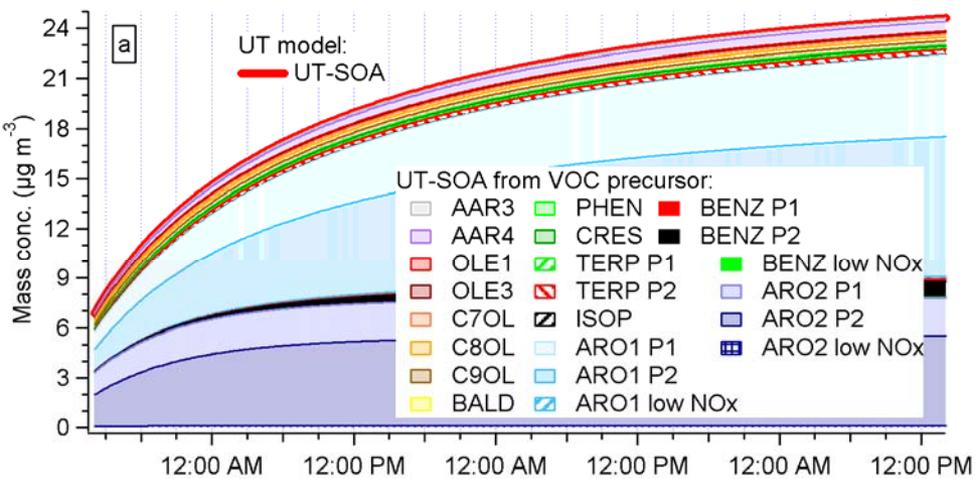
Figure SI-21
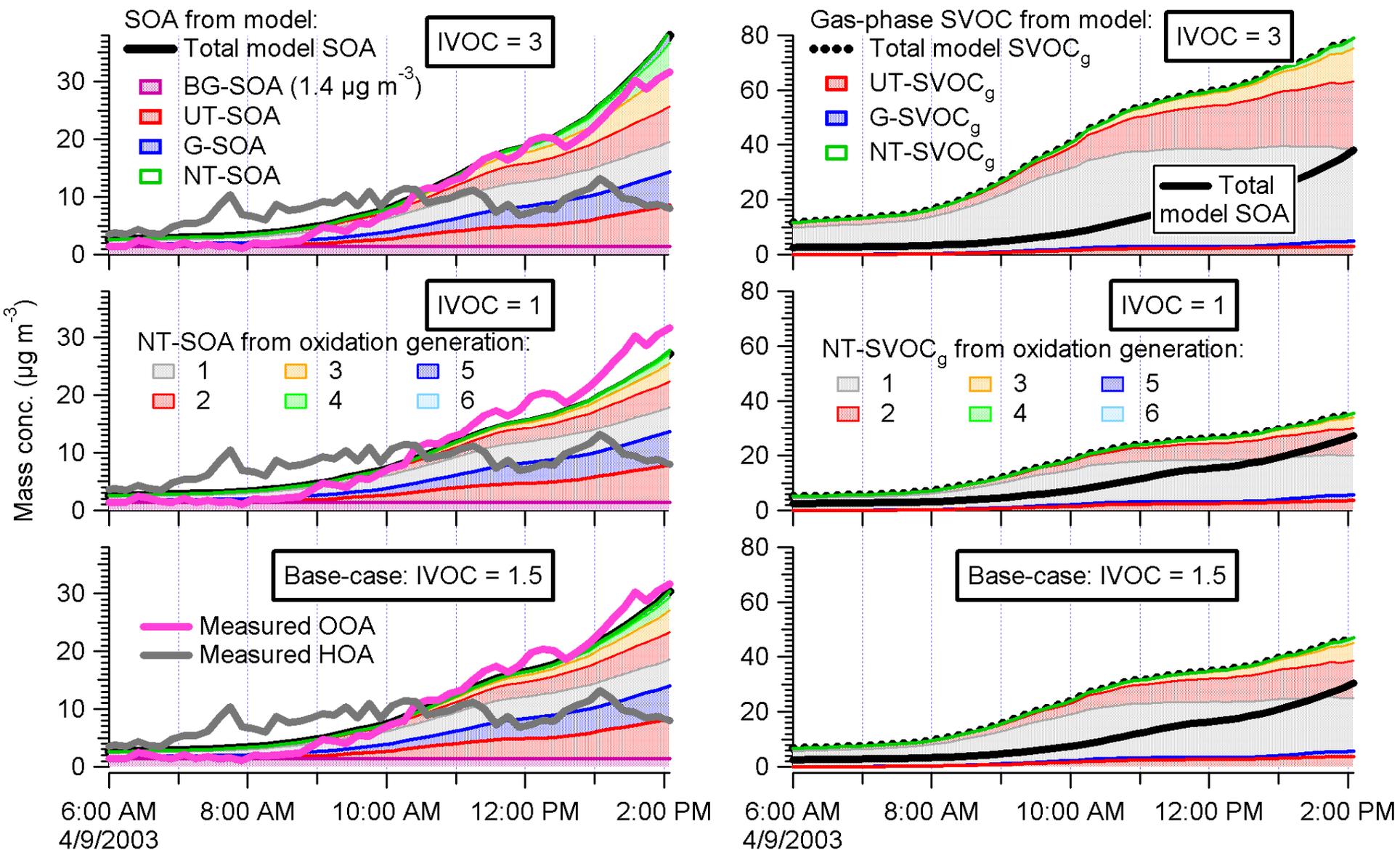
Figure SI-22
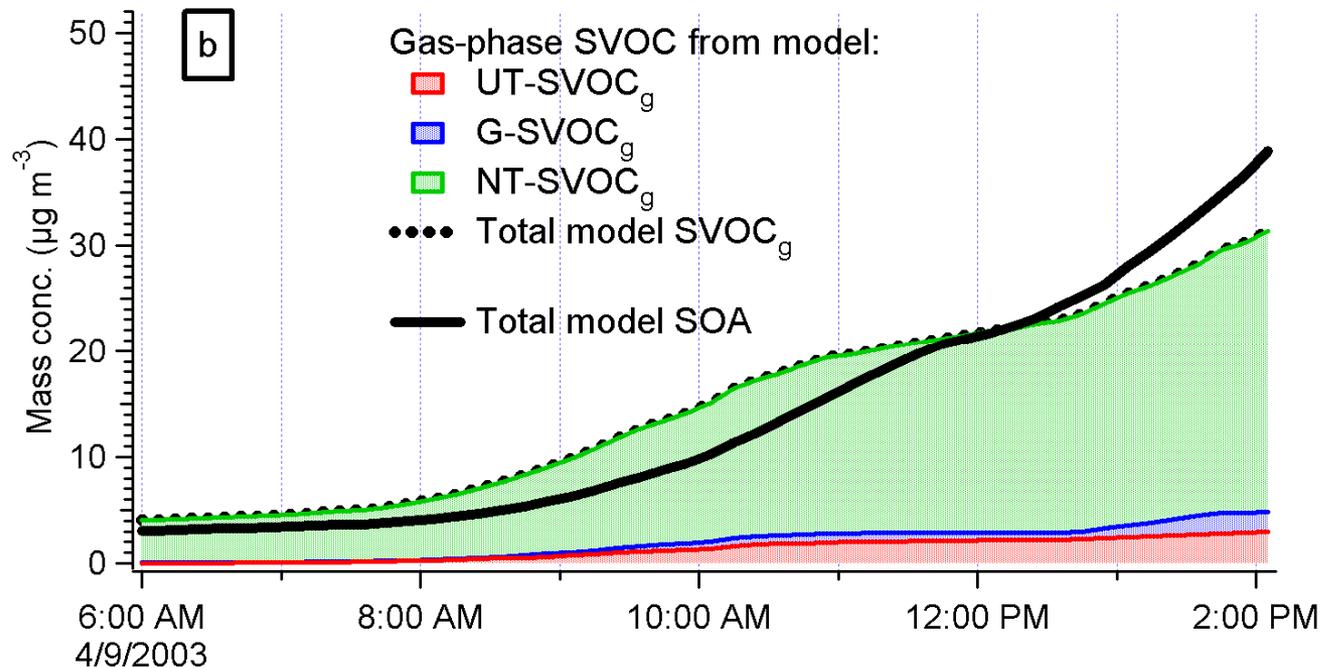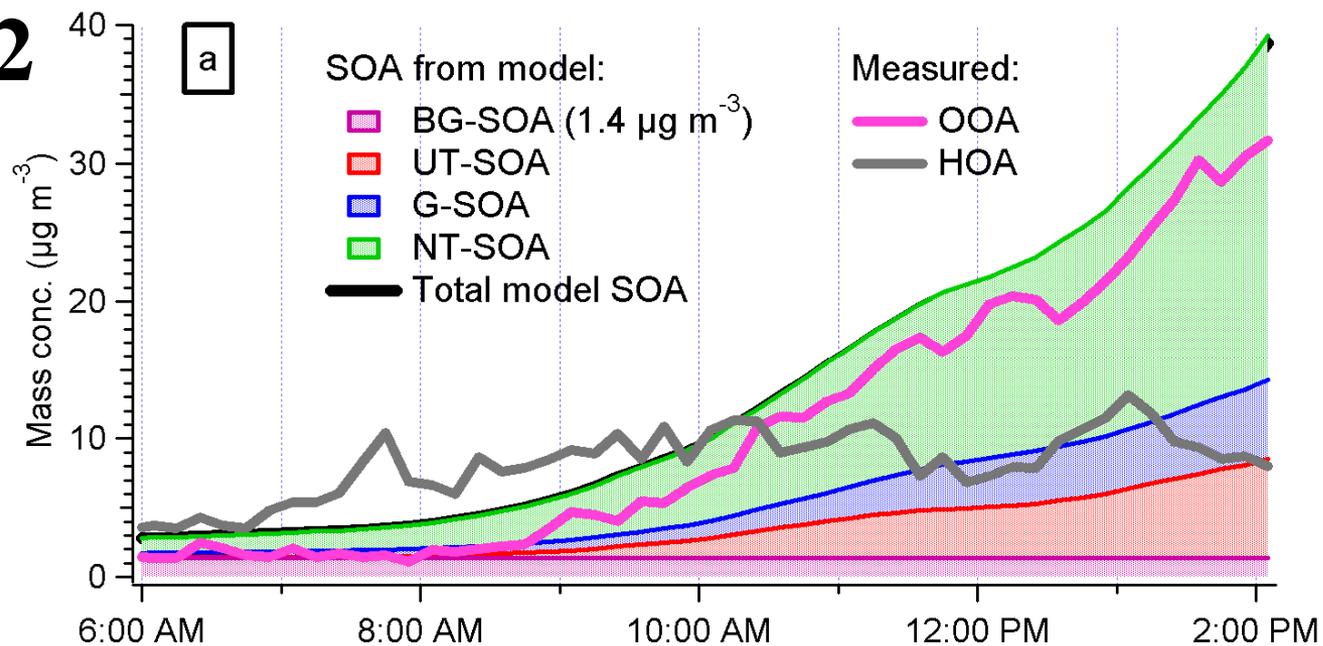
Figure SI-23
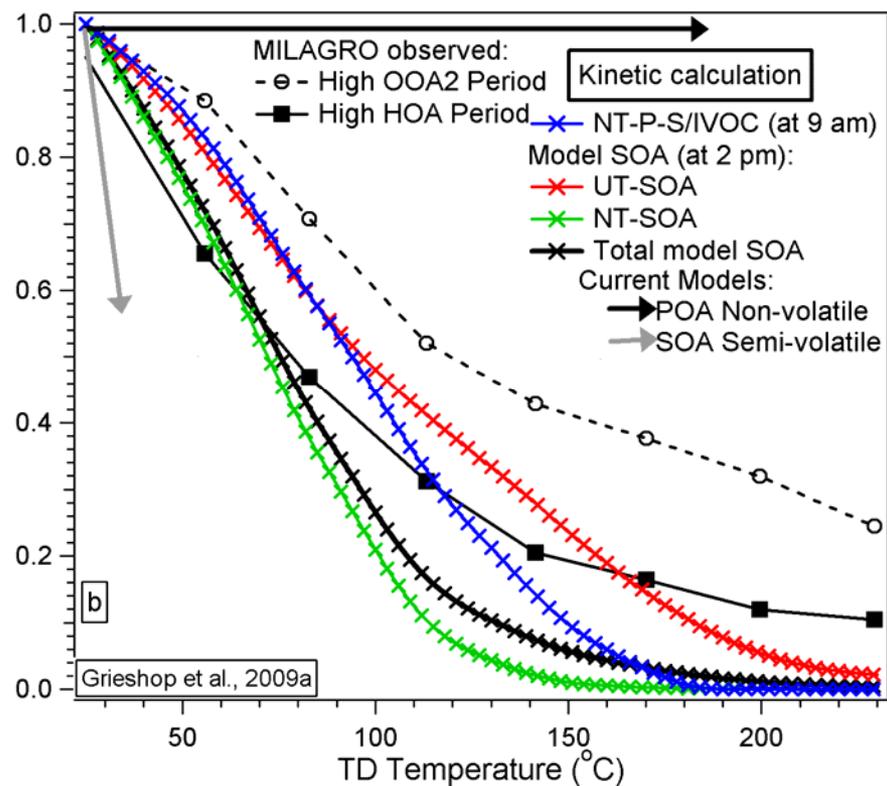
Figure SI-24

Figure SI-24

Figure SI-25
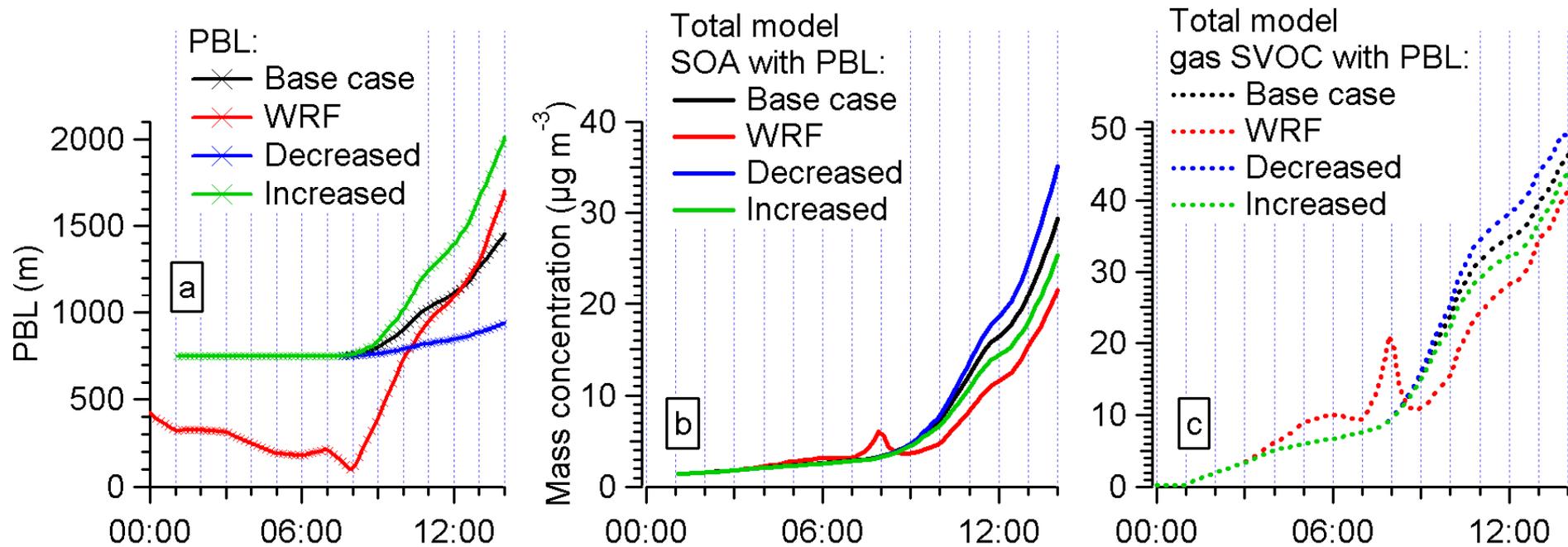
Figure SI-26

Figure SI-27

Figure SI-28